

Intensity Profile Projection: A Framework for Continuous-Time Representation Learning for Dynamic Networks

Alexander Modell, Ian Gallagher, Emma Ceccherini, Nick Whiteley, and Patrick Rubin-Delanchy

School of Mathematics, University of Bristol, UK

Abstract

We present a new algorithmic framework, Intensity Profile Projection, for learning continuous-time representations of the nodes of a dynamic network, characterised by a node set and a collection of instantaneous interaction events which occur in continuous time. Our framework consists of three stages: estimating the intensity functions underlying the interactions between pairs of nodes, e.g. via kernel smoothing; learning a projection which minimises a notion of intensity reconstruction error; and inductively constructing evolving node representations via the learned projection. We show that our representations preserve the underlying structure of the network, and are temporally coherent, meaning that node representations can be meaningfully compared at different points in time. We develop estimation theory which elucidates the role of smoothing as a bias-variance trade-off, and shows how we can reduce smoothing as the signal-to-noise ratio increases on account of the algorithm ‘borrowing strength’ across the network.

1 Introduction

Making sense of patterns of connections occurring over time is a common theme of modern data analysis and is often approached in one of two ways. On the one hand, we may see dynamic network data as a *graph*, in which connections between the same entities over time are somehow treated as one, e.g. through weighting. This view evokes methodological ideas such as community detection [1, 2], topological data analysis [3], or manifold learning [4, 5]. On the other, we may see the data as a set of *point processes* [6], each modelling the event times of connections between two entities. This view evokes temporal notions such as trend, changepoints and periodicity. There are many opportunities for innovation *combining ideas* from these different modelling cultures, a principle known more generally as the Medici effect [7].

In this paper, we develop a representation learning framework for continuous-time dynamic network data in which ideas from both the graph and temporal domains can be combined. Our framework has material advantages over existing approaches, broadly relating to statistical precision and interpretability, which open new possibilities for inference. For instance, in Section 4, we present a synthetic example involving continuously evolving network topology, which is shown to be hard to infer, not to say impossible, by other methods.

In more technical detail, we propose a family of procedures which return, for each node i , a low-dimensional vector-valued function $\widehat{X}_i(t)$ representing the node’s behaviour over time. By “precision”, above, we mean a uniform error bound: controlling the largest error of any representation over the entire time domain and node set. By “interpretability”, we are referring to a property of our method which to our knowledge is unique among continuous-time methods: two nodes at two points in time exhibiting statistically indistinguishable behaviour are mapped to the same position, up to noise. Properties known in the literature as temporal coherence (or longitudinal stability) and structure preservation (or cross-sectional stability) [8, 9] are established as special

cases in which the same node is considered at two distinct points in time, or two distinct nodes are considered at the same point in time. These results assume a generic inhomogeneous Poisson dynamic network model.

1.1 Related work

Our proposed framework combines ideas from point process modelling [10] and spectral embedding [11, 12]. The theoretical analysis draws on recent developments in entrywise eigenvector estimation for random matrices [13–16]. For a specific choice of intensity estimator (the histogram), our method can be viewed as a weighted graph analogue of Unfolded Spectral Embedding [9, 16], but those papers consider different data (multilayer or discrete time networks) and models.

We perform a comprehensive method comparison in Section 4. To our knowledge, the only unsupervised representation learning methods for dynamic network data (as defined in the next section) are [17–19], which are based on latent position models and have much weaker theoretical guarantees. There are a number of discrete-time dynamic network representation learning algorithms, which broadly fall under latent position models [20–22], spectral methods [9, 16, 23–25] and word-embedding-based [26, 27]. Given how limited the options are for handling continuous time, in our method comparison we also include some discrete-time methods which could reasonably be used as alternatives.

2 Intensity Profile Projection

Data. We consider dynamic network data, denoted \mathcal{G} , representing instantaneous undirected interactions between nodes over time, which we define formally as $\mathcal{G} = (\mathcal{V}, \mathcal{E})$ on a time domain $\mathcal{T} = (0, T]$, containing a vertex set $\mathcal{V} = [n]$ and a set of triples $\mathcal{E} = \{(i_e, j_e, t_e)\}_{e \geq 1}$, each corresponding to an undirected interaction event, where $i_e < j_e \in \mathcal{V}, t_e \in \mathcal{T}$. We let $\mathcal{E}_{ij} := \{t : (i, j, t) \in \mathcal{E}\}$ denote the interaction events between nodes i and j .

Model. We assume the interaction events \mathcal{E}_{ij} are driven by an independent inhomogeneous Poisson process with intensity $\lambda_{ij}(t)$. Informally:

$$\lambda_{ij}(t)dt = \mathbb{P}\{\text{interaction between nodes } i \text{ and } j \text{ in } (t, t + dt)\}.$$

We represent these intensities in a symmetric time-varying matrix $\mathbf{\Lambda}(\cdot) : \mathcal{T} \rightarrow \mathbb{R}_+^{n \times n}$.

Procedure. Intensity Profile Projection can be summarised as follows.

1. **Intensity estimation.** Construct intensity estimates $\widehat{\lambda}_{ij}(\cdot)$ of $\lambda_{ij}(\cdot)$ from \mathcal{E}_{ij} for all $i < j$.
2. **Subspace learning.** Compute the top d eigenvectors $\widehat{\mathbf{U}}_d = (\widehat{u}_1, \dots, \widehat{u}_d)$ of

$$\widehat{\mathbf{\Sigma}} := \frac{1}{T} \int_0^T \widehat{\mathbf{\Lambda}}^2(t) dt, \quad (1)$$

where $\widehat{\mathbf{\Lambda}}(t)$ has symmetric entries $\widehat{\lambda}_{ij}(t)$, and rows denoted $\widehat{\Lambda}_i(t)$ called *intensity profiles*.

3. **Projection.** For a query node i at time t , project the intensity profile $\widehat{\Lambda}_i(t)$ onto the subspace spanned by $\widehat{u}_1, \dots, \widehat{u}_d$, to obtain $\widehat{X}_i(t) = \widehat{\mathbf{U}}_d^\top \widehat{\Lambda}_i(t)$.

While we develop more principled statistical justifications for the procedure in future sections, it is inspired by a simple reconstruction argument. For an arbitrary d -dimensional subspace let

$$\widehat{r}_i(t; \mathbf{V}_d) := \left\| \mathbf{V}_d \mathbf{V}_d^\top \widehat{\Lambda}_i(t) - \widehat{\Lambda}_i(t) \right\|_2$$

Algorithm 1 Approximate Intensity Profile Projection

Input: Continuous time dynamic graph \mathcal{G} , dimension d .

- 1: Construct intensity estimates $\hat{\lambda}_{ij}(\cdot)$ of $\lambda_{ij}(\cdot)$ from \mathcal{E}_{ij} for all $i < j$.
- 2: Compute the top d left singular vectors $\hat{u}_1, \dots, \hat{u}_d$ of

$$\left[\hat{\Lambda}(t_1) \quad \hat{\Lambda}(t_2) \quad \cdots \quad \hat{\Lambda}(t_B) \right]$$

where $t_1 < \cdots < t_B$ are equally spaced points on $(0, T]$.

- 3: Define the trajectory of node i as

$$\hat{X}_i(t) := \hat{\mathbf{U}}_d^\top \hat{\Lambda}_i(t)$$

where $\hat{\mathbf{U}}_d := (\hat{u}_1, \dots, \hat{u}_d)$.

Output: Node trajectories $\hat{X}_1(t), \dots, \hat{X}_n(t)$.

denote the reconstruction error of node i at time t , where the columns of \mathbf{V}_d form an orthonormal basis of the subspace, and define the *integrated residual sum of squares* as

$$\hat{R}^2(\mathbf{V}_d) := \int_0^T \sum_{i=1}^n \hat{r}_i^2(t; \mathbf{V}_d) dt.$$

Lemma 1. *Among all d -dimensional subspaces of \mathbb{R}^n , $\hat{\mathbf{U}}_d$ minimises the integrated residual sum of squares criterion \hat{R}^2 .*

Lemma 1 may be viewed as a dynamic analogue to the classical Eckart-Young theorem on low-rank matrix approximation [28]. A proof is given in Section D of the appendix.

2.1 Intensity estimation

The choice of intensity estimator is left fully open, but our theory makes two important recommendations. First, there are computational gains to be made using sparse estimators for subspace learning. Second, the procedure borrows strength across the network, and can give precise representations even when the individual intensity estimates are noisy (e.g. inconsistent). In our experiments, we focus on standard non-parametric estimators such as the histogram or kernel smoothers, and choose kernels with finite support to induce sparse estimates.

2.2 Subspace learning

The subspace learning step of our procedure involves the computation of an integral, and computing the eigendecomposition of the resulting dense matrix $\hat{\Sigma}$, both of which may be infeasible for large networks. If a sparse intensity estimator is employed in step 1 of the procedure and we approximate the integral (1) using a numerical quadrature scheme, then step 2 can be rephrased as a single sparse, truncated singular value decomposition, which can be computed quickly for very large networks using an efficient solver [29, 30].

Consider the numerical approximation

$$\hat{\Sigma} \approx \frac{1}{B} \sum_{b=1}^B \hat{\Lambda}^2(t_b) \tag{2}$$

where $t_1 < \cdots < t_B$ are equally spaced points on $(0, T]$. The top d eigenvectors of the right-hand-side

of (2) are then equal¹ to the top d left singular vectors of the matrix

$$\left[\widehat{\Lambda}(t_1) \quad \widehat{\Lambda}(t_2) \quad \cdots \quad \widehat{\Lambda}(t_B) \right],$$

the row concatenation of $\widehat{\Lambda}(t_1), \dots, \widehat{\Lambda}(t_B)$. This procedure is presented in Algorithm 1.

2.3 Projection

The inductive nature of the Intensity Profile Projection allows us to obtain representations $\widehat{X}_i(t)$ on demand, for example, the full trajectory for a particular node, or the representations of the entire graph at a point in time. It is possible to obtain representations for intensity profiles outside the training sample, corresponding to new nodes or times outside the training domain, allowing online inference. In practice, one will need to retrain occasionally, i.e. return to step 2, although we leave the discussion of this computational and statistical trade-off for future work (see, for example, [31] in the context of static networks).

3 Estimation theory

In this section, we develop estimation theory showing the sense in which $\widehat{X}_i(t)$ is a “good” estimator of $X_i(t) := \mathbf{U}_d^\top \Lambda_i(t)$ where $\mathbf{U}_d = (u_1, \dots, u_d) \in \mathbb{R}^{n \times d}$ is the matrix containing the top- d orthonormal eigenvectors of

$$\Sigma := \frac{1}{T} \int_0^T \Lambda^2(t) dt.$$

In this section, we assume, without loss of generality, that $\mathcal{T} = (0, 1]$. We now introduce some quantities which appear in our main theorem. Firstly, we assume that each $\lambda_{ij}(\cdot)$ is Lipschitz with constant L , and is upper bounded by λ_{\max} . Secondly, we define the condition number and the eigengap,

$$\kappa := \frac{\sigma_1}{\sigma_d}, \quad \text{and} \quad \delta := \sigma_d - \sigma_{d+1},$$

respectively, where $\sigma_1^2 \geq \dots \geq \sigma_n^2$ are eigenvalues of Σ . Thirdly, we introduce the coherence parameter

$$\mu := \sqrt{\frac{n}{d}} \|\mathbf{U}_d\|_{2,\infty},$$

which is small when, informally, information about a single entry of Σ is “spread out” across the matrix [32]. Finally, we define the population residuals

$$r_i(t) := \|\mathbf{U}_d \mathbf{U}_d^\top \Lambda_i(t) - \Lambda_i(t)\|_2.$$

Rather than attempt to develop a theoretical framework encompassing all intensity estimators, we choose arguably the most rudimentary, the histogram, and we expect more powerful estimators will only improve matters. This choice of estimator is also attractive because it allows us pinpoint the crucial practical considerations at play.

Notation. We say an event E occurs *with overwhelming probability* if $\mathbb{P}(E) \geq 1 - n^{-c}$ for any constant $c > 0$. We use \ll, \gg, \lesssim and \gtrsim to denote inequalities which hide universal constants and, when qualified with the prior probabilistic statement, the constant c . Additionally, we write $a \asymp b$ if $a \lesssim b$ and $a \gtrsim b$.

We now state the assumptions we require for our theorem. Our first assumption is that the intensities bounded.

¹Up to signs, rotations in the eigenspaces in the case of repeated eigenvalues, and assuming a gap between the d th and $(d+1)$ th eigenvalues.

Assumption 1 (Bounded intensities). The intensities are upper bounded by a constant which doesn't depend on the other quantities in the problem; i.e. $\lambda_{\max} \lesssim 1$.

Our second assumption is a technical condition on the eigengap which, broadly speaking, ensures that there is “enough signal”.

Assumption 2 (Enough signal). The eigengap satisfies $\delta \log(\delta/\sqrt{n\lambda_{\max}}) \gtrsim \kappa n \lambda_{\max}$.

Our third assumption is on the population integrated residuals. It ensures that the intensity profiles $\Lambda_1(t), \dots, \Lambda_n(t)$ do not deviate “too much” from a common low-dimensional subspace.

Assumption 3 (Small population residuals). The population residuals satisfy $r_1(t), \dots, r_n(t) \lesssim \mu \sqrt{d\lambda_{\max}} \log^{5/2} n$ for all $t \in [0, 1]$.

Our final assumption is on the bin size, and ensures that the bins are not chosen “too small”.

Assumption 4 (Large enough bins). The number of bins satisfies $M \lesssim n\lambda_{\max}/\log^3 n$.

These assumptions are weaker than those typically required in the literature (e.g. on stochastic block models and random dot product graphs [2, 33]). We emphasize that we *do not* assume that Σ has low rank, and instead only require that the population residuals are sufficiently small that their contribution does not dominate our error bound.

As a special case, suppose that $\lambda_{ij}(t)$ are all of the same order of magnitude in the sense that $\lambda_{ij}(t) \asymp \rho$ for some $\rho \lesssim 1$ and all i, j, t , and that Σ has exactly rank d . Assumption 1 is automatically satisfied and one can show that $\delta \asymp n\rho$ and $\kappa \asymp 1$, implying that Assumption 2 is satisfied. The population residuals are all exactly zero, and Assumption 3 is satisfied. Assumption 4 requires that the expected number of events involving each node in each bin is at least of the order $\log^3 n$. This is analogous to the $\log n$ degree growth required for perfect clustering under the binary stochastic block model. Since the latter is an information-theoretic bound [34] and the additional logarithmic powers in our work stem from the sub-exponential tails of the Poisson distribution, we do not think this assumption can be weakened.

We now state our main theorem.

Theorem 1. *Suppose that $\hat{\lambda}_{ij}(t)$ are histogram estimates with M equally-spaced bins and that Assumptions 1-4 hold. Then with overwhelming probability, there exists an orthogonal matrix \mathbf{W} such that*

$$\max_{i \in [n]} \sup_{t \in (0,1)} \left\| \mathbf{W} \hat{X}_i(t) - X_i(t) \right\|_2 \lesssim \frac{n^{3/2} L \lambda_{\max}}{M \delta} + \mu \sqrt{M \lambda_{\max} d} \log^{5/2} n. \quad (3)$$

A proof of Theorem 1 is given in Section E of the appendix.

3.1 A bias-variance trade-off

The first term in the bound corresponds to the bias between $\bar{X}_i(t)$ and $X_i(t)$, where $\bar{X}_i(t)$ is a histogram approximation to $X_i(t)$ (modulo orthogonal transformation, see Section E.4 of the appendix). The second term corresponds to the variance of the estimate.

Theorem 1 gives some theoretical guidance on how select the number of bins in the histogram estimator. For simplicity, consider the setting where $\lambda_{ij}(t) \asymp \rho$ are all of the same order of magnitude (so that $\delta \asymp n\rho$ and $\kappa \asymp 1$), the Lipschitz constant $L \asymp \rho L_0$ scales with the intensities, and μ and d are fixed. Then, ignoring logarithmic terms in n , the bound in (3) is optimised by choosing

$$M \asymp (n\rho L_0^2)^{1/3}.$$

Figure 1 illustrates this bias-variance trade-off with an example. We simulate a dynamic network with 100 nodes with common intensities $\lambda_{ij}(t) = 0.7 \times \{2 + \cos(t)\}$, for all i, j , on the time domain $(0, 4\pi]$.

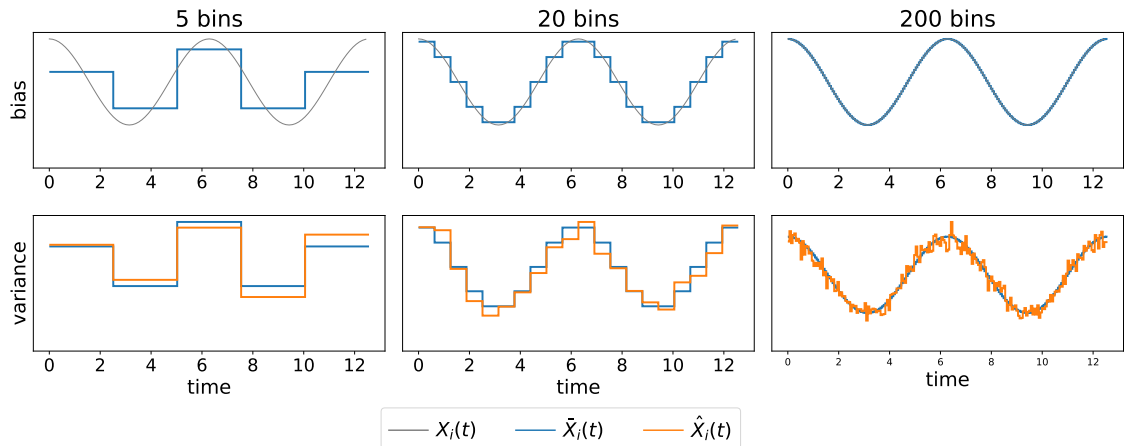


Figure 1: A bias-variance trade-off. We simulate a network with common intensities $\lambda_{ij}(t) = 0.7 \times \{2 + \cos(t)\}$ for all i, j , and apply Intensity Profile Projection with a histogram intensity estimator with 5, 20, and 200 bins. In the ‘bias’ plots, the gray lines shows an estimand $X_i(t)$, while the blue lines shows its histogram approximation. The discrepancy between the gray line and the blue line corresponds the bias of the Intensity Profile Projection estimator. In the ‘variance’ plots, the blues lines are as in the ‘bias’ plots and the orange line show the estimate obtains using Intensity Profile Projection into one dimension. The discrepancy between the blue line and the orange line corresponds the variance of the Intensity Profile Projection estimator.

The top row shows the population representation $X_i(t)$ of a single node (gray) and its histogram approximation $\bar{X}_i(t)$ (blue) for a variety of bin sizes. The more bins that are chosen, the smaller the bias and the more $\bar{X}_i(t)$ resembles $X_i(t)$. The bottom rows shows the histogram approximation $\bar{X}_i(t)$, and the estimate $\hat{X}_i(t)$ (orange) obtained using Intensity Profile Projection. The fewer bins that are chosen, the smaller the variance and the more that $\hat{X}_i(t)$ resembles $\bar{X}_i(t)$.

4 Structure preservation and temporal coherence

For many practical inference tasks, it is desirable for a representation learning procedure to possess the following two properties:

- **Structure preserving.** If two nodes exhibit statistically indistinguishable behaviour at a given time, then their representations at that time are similar. That is, if $\Lambda_i(t) = \Lambda_j(t)$, then $\hat{X}_i(t) \approx \hat{X}_j(t)$;
- **Temporally coherent.** If a node exhibits statistically indistinguishable behaviour at two distinct points in time, then its representations at both these times are similar. That is, if $\Lambda_i(s) = \Lambda_i(t)$, then $\hat{X}_i(s) \approx \hat{X}_i(t)$.

It has been observed in a recent survey of [8] that almost all existing dynamic network embedding procedures possess only one of these properties, but not both.

In the following lemma, we formally define $\hat{X}_i(s) \approx \hat{X}_j(t)$ to mean that $X_i(s) = X_j(t)$, referring to equality “up to statistical noise” in the sense of Theorem 1.

Lemma 2. *Intensity Profile Projection is both structure preserving and temporally coherent.*

This follows from the simple observation that $X_i(t)$ is a fixed function of $\Lambda_i(t)$ for all i and t . To the best of our knowledge, Intensity Profile Projection is the only existing continuous-time procedure which satisfies these desiderata.

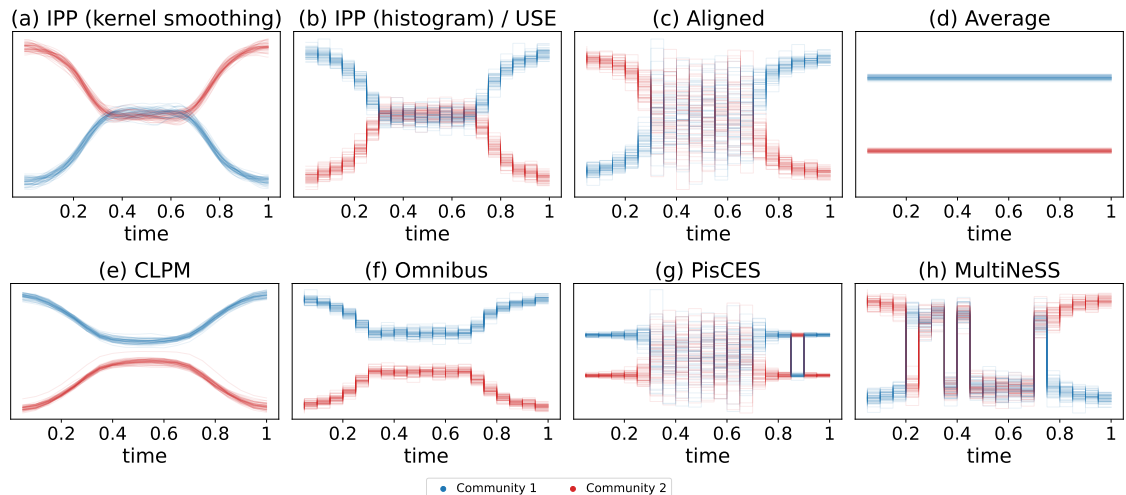


Figure 2: One-dimensional PCA visualisation of the two-dimensional node representations, obtained using a collection of methods, for a network simulated from a bifurcating block model. Colours correspond to the community membership of the node.

4.1 Simulated example: a bifurcating block model

To illustrate these properties, we simulate a two-community dynamic stochastic block model (i.e. where $\mathbf{A}(t)$ is block structured) in which the intra-community intensities and inter-community intensities are initially distinct, they then gradually merge, remain indistinguishable for some time, and finally diverge. We refer to this model as a *bifurcating block model* and provide full details of the simulation in the supplementary materials.

We apply Intensity Profile Projection to the simulated network, using both a histogram intensity estimator, and a kernel smoother, to produce two-dimensional representations. For visualisation, we reduce the dimension from two to one using a dynamic adaptation of principal component analysis (see Section C of the appendix), and the resulting representations are shown in Figures 2(a) and (b).

In both cases, the estimated trajectories mirror the underlying dynamics of the network: the two communities are in well separated to begin with, gradually merge, remain relatively constant before returning to the positions in which they started.

We now illustrate the potential pitfalls of some more naive approaches for embedding dynamic networks. We find that most existing methodology can be viewed as some combination of the two techniques:

- **Alignment.** Obtain a sequence of static snapshots of the network, embed each of the networks snapshots separately and subsequently align the embedding from window $t + 1$ with the embedding from window t .
- **Averaging.** Obtain a static summary of the network by averaging it over time, and to embed this to obtain constant node representations.

Alignment preserves the structure of the network at each point in time, however can fail to be temporally coherent. Averaging is temporally coherent, but can fail to preserve the structure of the network. To illustrate this point, we apply both approaches, using adjacency spectral embedding into two dimensions, orthogonal Procrustes alignment and linear interpolation, to a network simulated from the bifurcating block model. Figures 2(c) and (d) show visualisations of the trajectories obtained from each approach.

4.2 Method comparison

In this section, we demonstrate how our procedure compares to some existing methods on the simulated data described above. Due to the limited number of continuous-time methods, we include a number of discrete-time methods (Omnibus, PisCSE and MultiNeSS) which we give as an input a discrete sequence of snapshots $\mathbf{A}(1), \dots, \mathbf{A}(M)$ of our simulated continuous-time networks. We compare the following methods:

- **IPP (kernel smoothing)**. Algorithm 1 applied with intensities estimated using kernel smoothing.
- **IPP (histogram) / USE** [16]. Algorithm 1 applied with intensities estimated using a histogram estimator. Equivalent to a weighted extension of the Unfolded Spectral Embedding algorithm of [16].
- **CLPM** [17]. Fits a continuous latent position model $\log \lambda_{ij}(t) = \beta - \|Z_i(t) - Z_j(t)\|^2$ with a penalty on large velocities in the latent space.
- **Omnibus** [23]. Approximately factorises the matrix \mathbf{A} with blocks $\mathbf{A}[k, l] = \frac{1}{2}(\mathbf{A}(k) + \mathbf{A}(l))$, using a spectral decomposition.
- **PisCES** [24]. Minimises the objective function

$$\sum_{k=1}^M \|\mathbf{L}(k) - \mathbf{L}^*(k)\|_F^2 + \alpha \sum_{k=1}^{M-1} \|\mathbf{L}^*(k) - \mathbf{L}^*(k+1)\|_F^2,$$

for $\mathbf{L}^*(1), \dots, \mathbf{L}^*(M)$, where $\alpha \in [0, 1]$ and $\mathbf{L}(k)$ are the Laplacian normalisations of $\mathbf{A}(k)$. Then, approximately factorises each $\mathbf{L}^*(1), \dots, \mathbf{L}^*(M)$ using spectral decompositions.

- **MultiNeSS** [35]. Fits a latent position model $\mathbf{A}_{ij}(k) \sim Q\{\cdot; f(Z_i(k), Z_j(k)), \phi\}$, where $Q(\cdot; \theta, \phi)$ is a parametric distribution.

We use an embedding dimension of $d = 2$ for all methods, and for visualisation we reduce this to one using PCA. Additional details such as hyperparameter selection, where applicable, are given in the Section A of the appendix.

The CLPM and Omnibus methods produce representations which are temporally coherent, however both fail to capture the complete merging of the communities, shown by Figures 2(e) and (f), and are therefore not structure preserving. The PisCES and MultiNeSS methods produce representations which are structure preserving, however both are unstable when the communities are indistinguishable, shown by Figures 2(g) and (h), and are therefore not temporally coherent.

5 Real data

We demonstrate Intensity Profile Projection on a dataset containing the face-to-face interactions of the pupils of a primary school in Lyon over two days in October 2009 [36]. During the study, discreet radio-frequency identification devices were worn by 232 pupils and 10 teachers which recorded their face-to-face interactions. When two participants were in close proximity over an interval of 20 seconds, the timestamped interaction event was recorded. The school contains five year groups, each divided into two classes, and each class has an assigned room and an assigned teacher. The school day runs from 8:30am to 4:30pm, with a lunch break from 12:00pm to 2:00pm, and no data was gathered on contacts taking place outside the school or during sports activities. For more details about the study and dataset, we refer the reader to [36].

We apply Intensity Profile Projection to the data corresponding to each day of the study using a kernel smoother with an Epanechnikov kernel, choosing a bandwidth of 5 minutes and computing 30 dimensional trajectories.

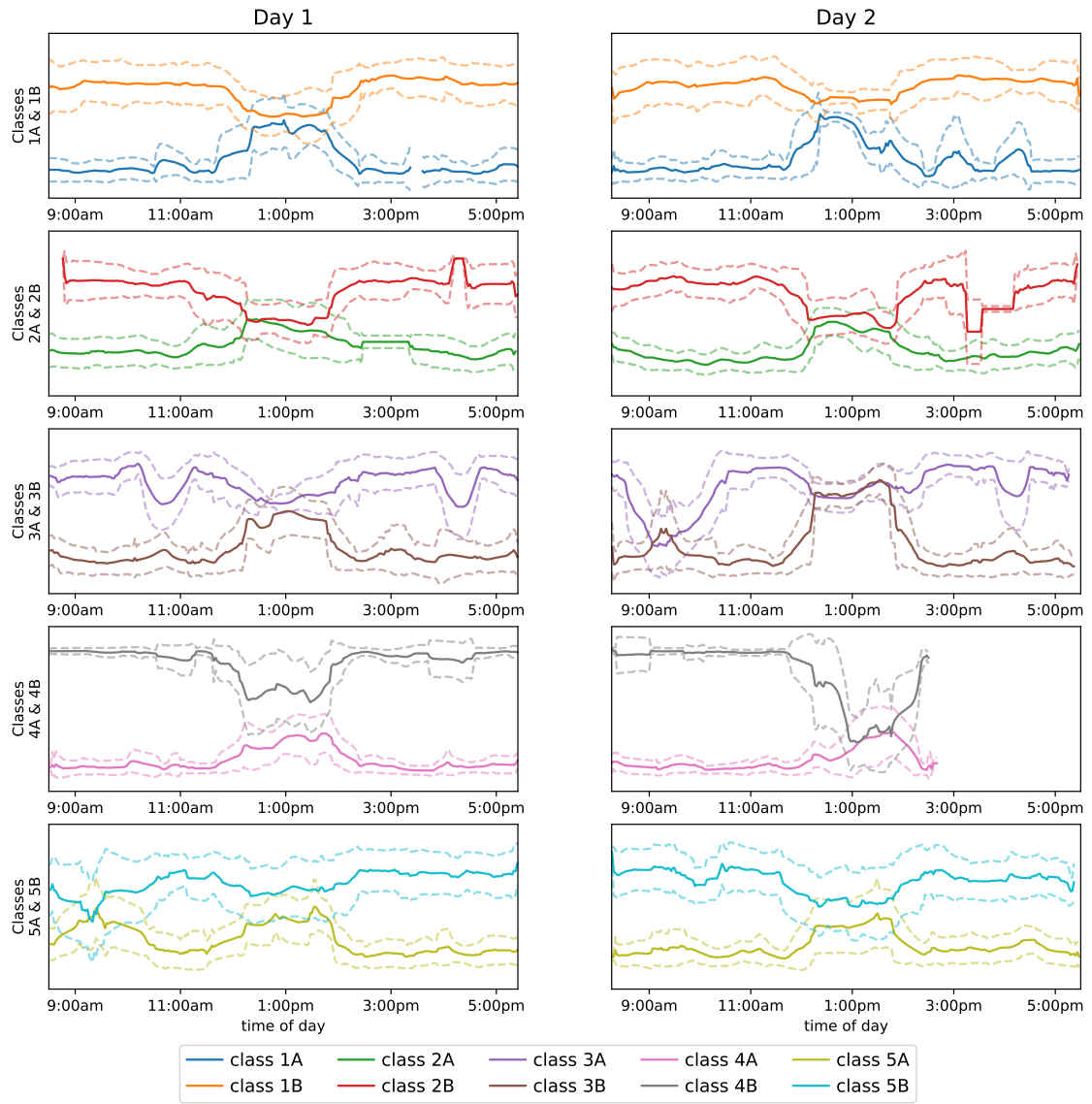


Figure 3: One-dimensional PCA visualisation of the 30-dimensional node representations for pairs of classes in the same year group. The solid lines show the average trajectory for each class, and the dashed line show one standard deviation above and below.

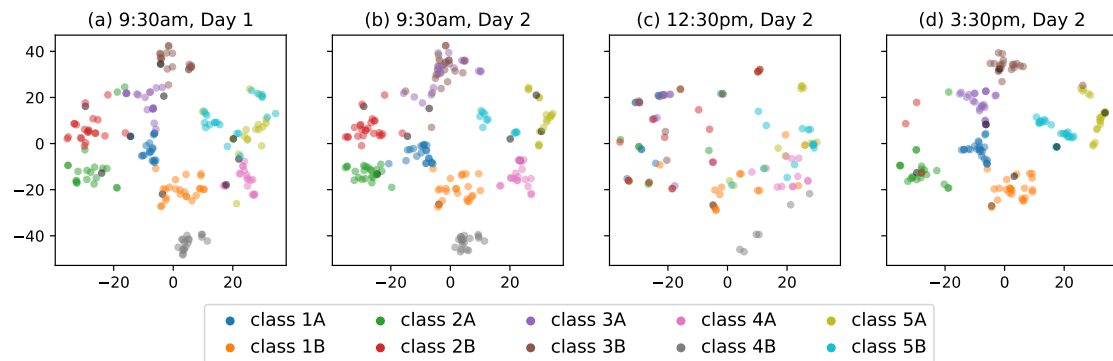


Figure 4: Two-dimensional t-SNE visualisation of the 30-dimensional node representations of all pupils and teachers evaluated at 9:30am on Day 1, and 9:30am, 12:30pm and 3:30pm on Day 2.

To visualise the node trajectories, we first rescale them to have unit norm, which has the effect of removing information about the “activeness” of a node from its representation (see, for example, [37]), and apply two dimension reduction techniques. The first is principal component analysis (PCA), which we adapt to our dynamic setting by projecting the (centered) representations onto the the direction of maximum average variance over the time domain. This visualisation gives us a temporally coherent view on the trajectories (more details are given in Section C of the appendix). In Figure 3, we visualise the trajectories of each pair of classes in each year group using PCA, and for clarity, we just plot the average trajectory for each class, along with one standard deviation above and below.

The second is t-Distributed Stochastic Neighbor Embedding (t-SNE), a popular non-linear dimension-reduction tool which provides enough flexibility to visualise the whole set of representations at each point in time. Figure 4 shows t-SNE visualisations of the node representations at a collection of times throughout the study.

Figure 3 clearly shows the mixing of classes during the lunch hours, and from Figures 4, we see that the the representations are much more fragmented during the lunch hour (12:30pm, Day 2) than they are during lessons at the other times, where they form tighter clusters corresponding to classes.

While it is reassuring that the geometry of the trajectories reflects the *known* class and timetable structures of the school, it also allows us to uncover structure in the data that *was not known* from the report on the study. For example, classes 5A and 5B (olive and cyan, respectively) merge into a single cluster at approximately 9:30am on Day 1, and classes 3A and 3B (brown and pink, respectively) do the same at approximately 9:30am on Day 2. One might conjecture that this corresponds to a joint lesson, which is taken by the students of both classes in a year group.

6 Discussion

We have presented an algorithmic framework to learn continuous-time, low-dimensional trajectories representing the evolving behaviours of nodes in a dynamic network.

A limitation of our framework is the need for bandwidth and dimension selection. These decisions are difficult because they are trade-offs, bias versus variance in the case of bandwidth selection (as seen here), and statistical versus computational in the case of dimension selection (see e.g. [38]). In the presence of a specific supervised downstream task, both decisions could be assisted by cross-validation. In unsupervised settings with reasonably-sized networks, our method is very fast, allowing expedient exploration of different choices.

Our method might be viewed as a dynamic analogue of adjacency spectral embedding for static graphs [39] and, as result, in future research it could be profitable to find dynamic analogues of others variants of spectral embedding, e.g. applying Laplacian normalisation [40–42] or regularisation [37, 43].

We view our framework as providing a platform on which novel inference procedures can be developed, particularly combining graph and temporal concepts. For example, in dynamic networks with continuously evolving community structure, it might be interesting to develop procedures for detecting branching points (see bifurcating block model example, Section 4), or measures of polarisation and cohesion in the network via the velocities of the trajectories. More generally, we believe there is much left to understand and exploit in the time-evolving topology and geometry of these representations.

We believe improved dynamic network analysis can be used for societal good, in applications such as cyber-security, or combating human-trafficking, fraud, and corruption. However, one should also be aware of the risks, particularly to individual privacy and targeted influence.

References

- [1] Mark EJ Newman. Modularity and community structure in networks. *Proceedings of the national academy of sciences*, 103(23):8577–8582, 2006.
- [2] Emmanuel Abbe. Community detection and stochastic block models: recent developments. *The Journal of Machine Learning Research*, 18(1):6446–6531, 2017.
- [3] Larry Wasserman. Topological data analysis. *Annual Review of Statistics and Its Application*, 5:501–532, 2018.
- [4] Patrick Rubin-Delanchy. Manifold structure in graph embeddings. *Advances in Neural Information Processing Systems*, 33:11687–11699, 2020.
- [5] Avanti Athreya, Minh Tang, Youngser Park, and Carey E. Priebe. On estimation and inference in latent structure random graphs. *Statistical Science*, 36(1):68 – 88, 2021. doi: 10.1214/20-STS787. URL <https://doi.org/10.1214/20-STS787>.
- [6] Patrick O Perry and Patrick J Wolfe. Point process modelling for directed interaction networks. *Journal of the Royal Statistical Society: SERIES B: Statistical Methodology*, pages 821–849, 2013.
- [7] Frans Johansson. *The Medici Effect, with a new preface and discussion guide: what elephants and epidemics can teach us about innovation*. Harvard Business Review Press, 2017.
- [8] Guotong Xue, Ming Zhong, Jianxin Li, Jia Chen, Chengshuai Zhai, and Ruochen Kong. Dynamic network embedding survey. *Neurocomputing*, 472:212–223, 2022.
- [9] Ian Gallagher, Andrew Jones, and Patrick Rubin-Delanchy. Spectral embedding for dynamic networks with stability guarantees. *Advances in Neural Information Processing Systems*, 34: 10158–10170, 2021.
- [10] Peter Diggle. A kernel method for smoothing point process data. *Journal of the Royal Statistical Society: Series C (Applied Statistics)*, 34(2):138–147, 1985.
- [11] Avanti Athreya, Carey E Priebe, Minh Tang, Vince Lyzinski, David J Marchette, and Daniel L Sussman. A limit theorem for scaled eigenvectors of random dot product graphs. *Sankhya A*, 78:1–18, 2016.
- [12] Patrick Rubin-Delanchy, Joshua Cape, Minh Tang, and Carey E Priebe. A statistical interpretation of spectral embedding: the generalised random dot product graph. *Journal of the Royal Statistical Society Series B: Statistical Methodology*, 84(4):1446–1473, 2022.
- [13] Emmanuel Abbe, Jianqing Fan, Kaizheng Wang, and Yiqiao Zhong. Entrywise eigenvector analysis of random matrices with low expected rank. *Annals of statistics*, 48(3):1452, 2020.
- [14] Lihua Lei. Unified $\ell_{2 \rightarrow \infty}$ eigenspace perturbation theory for symmetric random matrices. *arXiv preprint arXiv:1909.04798*, 2019.
- [15] Fangzheng Xie. Entrywise limit theorems of eigenvectors and their one-step refinement for sparse random graphs. *arXiv preprint arXiv:2106.09840*, 2021.
- [16] Andrew Jones and Patrick Rubin-Delanchy. The multilayer random dot product graph. *arXiv preprint arXiv:2007.10455*, 2020.
- [17] Riccardo Rastelli and Marco Corneli. Continuous latent position models for instantaneous interactions. *arXiv preprint arXiv:2103.17146*, 2021.
- [18] Abdulkadir Çelikkanat, Nikolaos Nakis, and Morten Mørup. Piecewise-velocity model for learning continuous-time dynamic node representations. *arXiv preprint arXiv:2212.12345*, 2022.

- [19] Igor Artico and Ernst Wit. Fast inference of latent space dynamics in huge relational event networks. *arXiv preprint arXiv:2303.17460*, 2023.
- [20] Purnamrita Sarkar and Andrew W Moore. Dynamic social network analysis using latent space models. *Advances in neural information processing systems*, 18:1145, 2006.
- [21] Daniel K Sewell and Yuguo Chen. Latent space models for dynamic networks. *Journal of the american statistical association*, 110(512):1646–1657, 2015.
- [22] Nial Friel, Riccardo Rastelli, Jason Wyse, and Adrian E Raftery. Interlocking directorates in Irish companies using a latent space model for bipartite networks. *Proceedings of the National Academy of Sciences*, 113(24):6629–6634, 2016.
- [23] Keith Levin, Avanti Athreya, Minh Tang, Vince Lyzinski, Youngser Park, and Carey E Priebe. A central limit theorem for an omnibus embedding of multiple random graphs and implications for multiscale network inference. *arXiv preprint arXiv:1705.09355*, 2017.
- [24] Fuchen Liu, David Choi, Lu Xie, and Kathryn Roeder. Global spectral clustering in dynamic networks. *Proceedings of the National Academy of Sciences*, 115(5):927–932, 2018.
- [25] Joshua Cape. Spectral analysis of networks with latent space dynamics and signs. *Stat*, 10(1): e381, 2021.
- [26] Lun Du, Yun Wang, Guojie Song, Zhicong Lu, and Junshan Wang. Dynamic network embedding: An extended approach for skip-gram based network embedding. In *IJCAI*, volume 2018, pages 2086–2092, 2018.
- [27] Sedigheh Mahdavi, Shima Khoshraftar, and Aijun An. dynnode2vec: Scalable dynamic network embedding. In *2018 IEEE International Conference on Big Data (Big Data)*, pages 3762–3765. IEEE, 2018.
- [28] Carl Eckart and Gale Young. The approximation of one matrix by another of lower rank. *Psychometrika*, 1(3):211–218, 1936.
- [29] Richard Bruno Lehoucq. *Analysis and implementation of an implicitly restarted Arnoldi iteration*. Rice University, 1995.
- [30] James Baglama and Lothar Reichel. Augmented implicitly restarted Lanczos bidiagonalization methods. *SIAM Journal on Scientific Computing*, 27(1):19–42, 2005.
- [31] Keith Levin, Fred Roosta, Michael Mahoney, and Carey Priebe. Out-of-sample extension of graph adjacency spectral embedding. In *International Conference on Machine Learning*, pages 2975–2984. PMLR, 2018.
- [32] Emmanuel Candes and Benjamin Recht. Exact matrix completion via convex optimization. *Communications of the ACM*, 55(6):111–119, 2012.
- [33] Avanti Athreya, Donniell E Fishkind, Minh Tang, Carey E Priebe, Youngser Park, Joshua T Vogelstein, Keith Levin, Vince Lyzinski, and Yichen Qin. Statistical inference on random dot product graphs: a survey. *The Journal of Machine Learning Research*, 18(1):8393–8484, 2017.
- [34] Emmanuel Abbe and Colin Sandon. Community detection in general stochastic block models: Fundamental limits and efficient algorithms for recovery. In *2015 IEEE 56th Annual Symposium on Foundations of Computer Science*, pages 670–688. IEEE, 2015.
- [35] Peter W MacDonald, Elizaveta Levina, and Ji Zhu. Latent space models for multiplex networks with shared structure. *Biometrika*, 109(3):683–706, 2022.
- [36] Juliette Stehlé, Nicolas Voirin, Alain Barrat, Ciro Cattuto, Lorenzo Isella, Jean-François Pinton, Marco Quaggiotto, Wouter Van den Broeck, Corinne Régis, Bruno Lina, et al. High-resolution measurements of face-to-face contact patterns in a primary school. *PloS one*, 6(8): e23176, 2011.

- [37] Tai Qin and Karl Rohe. Regularized spectral clustering under the degree-corrected stochastic blockmodel. *Advances in neural information processing systems*, 26, 2013.
- [38] Matthias Löffler, Anderson Y Zhang, and Harrison H Zhou. Optimality of spectral clustering in the gaussian mixture model. *The Annals of Statistics*, 49(5):2506–2530, 2021.
- [39] Daniel L Sussman, Minh Tang, Donniell E Fishkind, and Carey E Priebe. A consistent adjacency spectral embedding for stochastic blockmodel graphs. *Journal of the American Statistical Association*, 107(499):1119–1128, 2012.
- [40] Fan RK Chung. *Spectral graph theory*, volume 92. American Mathematical Soc., 1997.
- [41] Ulrike Von Luxburg. A tutorial on spectral clustering. *Statistics and computing*, 17:395–416, 2007.
- [42] Minh Tang and Carey E Priebe. Limit theorems for eigenvectors of the normalized laplacian for random graphs. *The Annals of Statistics*, 46(5):2360–2415, 2018.
- [43] Yilin Zhang and Karl Rohe. Understanding regularized spectral clustering via graph conductance. *Advances in Neural Information Processing Systems*, 31, 2018.
- [44] Francesco Sanna Passino, Nicholas A Heard, and Patrick Rubin-Delanchy. Spectral clustering on spherical coordinates under the degree-corrected stochastic blockmodel. *Technometrics*, 64(3):346–357, 2022.
- [45] Laurens Van der Maaten and Geoffrey Hinton. Visualizing data using t-sne. *Journal of machine learning research*, 9(11), 2008.
- [46] George C Linderman, Manas Rachh, Jeremy G Hoskins, Stefan Steinerberger, and Yuval Kluger. Fast interpolation-based t-sne for improved visualization of single-cell rna-seq data. *Nature methods*, 16(3):243–245, 2019.
- [47] Jianqing Fan, Weichen Wang, and Yiqiao Zhong. An ℓ_∞ eigenvector perturbation bound and its application to robust covariance estimation. *Journal of Machine Learning Research*, 18(207):1–42, 2018.
- [48] Stanislav Minsker. On some extensions of bernstein’s inequality for self-adjoint operators. *Statistics & Probability Letters*, 127:111–119, 2017.
- [49] Afonso S Bandeira and Ramon Van Handel. Sharp nonasymptotic bounds on the norm of random matrices with independent entries. *Annals of Probability*, 44(4):2479–2506, 2016.
- [50] Yuxin Chen, Yuejie Chi, Jianqing Fan, Cong Ma, et al. Spectral methods for data science: A statistical perspective. *Foundations and Trends® in Machine Learning*, 14(5):566–806, 2021.
- [51] David Pollard. Empirical processes: Theory and applications. In *NSF-CBMS Regional Conference Series in Probability and Statistics*, pages i–86. JSTOR, 1990.

Appendix

A Details of the simulated example and method comparison of Sections 4.1 and 4.2

We simulate data according to the following generative process, which might be viewed as describing as a dynamic, two-community stochastic block model. Assign to each node i a variable $z_i \in \{1, 2\}$ denoting its community (which does not change with time). If nodes i and j are in the same community, i.e., $z_i = z_j$, the point process \mathcal{E}_{ij} follows a homogeneous Poisson process with (fixed) intensity k . Otherwise, \mathcal{E}_{ij} follows an inhomogeneous Poisson process with intensity

$$\lambda_{ij}(t) = \begin{cases} k \exp\{\lambda(t - s_1)\} & t < s_1, \\ k & s_1 \leq t < s_2, \\ k \exp\{-\lambda(t - s_2)\} & t \geq s_2, \end{cases}$$

where $0 < s_1 < s_2 < T$. This model describes two communities gradually coming together until fully merging by time s_1 , before splitting at time s_2 and then gradually drifting apart. We simulate from this model using the parameters $T = 1$, $n = 100$, $z_1, \dots, z_{50} = 1$, $z_{51}, \dots, z_{100} = 2$, $\lambda = 10$, $k = 100$, $s_1 = 0.3$ and $s_2 = 0.7$.

In our method comparison, we used an embedding dimension of $d = 2$ for all methods, unless otherwise stated. For the discrete time methods, we construct a series of 20 snapshots of the continuous-time network, each a weighted static networks whose edge weights are the number of events which occur on the edge in the corresponding time window. Selection of hyperparameters and compute time (on a Dell Latitude 5431 with an Intel Core i7-1270P processor) for each method is outlined below:

- **Intensity Profile Projection (histogram)**: We used a bin size of $\frac{1}{M} = \frac{1}{20}$. The computation takes approximately 8 seconds.
- **Intensity Profile Projection (kernel smoothing)**: We used a Epanechnikov kernel with bandwidth 0.1 and applied the approximate Intensity Profile Projection algorithm with $B = 20$. Different values of bandwidth gave similar results in terms of embedding structure; we chose this bandwidth to achieve the desired smoothness. The computation takes approximately 17 seconds.
- **Aligned adjacency spectral embedding**: The computation takes less than 1 second.
- **Average adjacency spectral embedding**: The computation takes approximately 1 second.
- **CLPM** [17]: The dimension is automatically computed by the algorithm as $d = 2$. The hyperparameters are chosen equal to the ones used in ‘‘Simulation C’’ in [17] which is a similar simulated example with two communities. We used 19 changes point which correspond to 20 windows. The implementation was obtained from the Github repository <https://github.com/marcogenni/CLPM>. The computation takes approximately 480 seconds.
- **Omnibus** [23]: The computation takes approximately 1 second.
- **PisCES** [24]: The dimension is automatically selected by the algorithm as $d = 2$. The smoothing parameter is chosen with cross-validation which results in equivalent log-likelihood values for α from 0.00001 to 0.001. We choose $\alpha = 0.001$ which is the larger value for which the algorithm converges. The implementation was obtained from the Github repository <https://github.com/xuranw/PisCES>. The computation takes less than 1 second.

- **MultiNeSS** [35]: The dimension is automatically selected by the algorithm as $d = 2$ for all windows except windows 5 to 16 for which $d = 1$ is selected. For these windows, we set missing the second dimension to zeros. The implementation is obtained from the `multiness` R package (available on CRAN) and hyperparameters are set to their default values. The computation takes less than 1 second.

B Additional real data analysis

We provide further experiments and details of the Intensity Profile Projection analysis of the Lyon primary school dataset described in Section 5. As a comparison to the analysis in the paper, we apply Intensity Profile Projection to the data corresponding to each day of the study with a histogram intensity estimator, choosing a bin size of 10 minutes and computing 30 dimensional trajectories.

Figure 7 (equivalent to Figure 3) visualises the trajectories of each pair of classes in each year group using PCA where we plot the average trajectory for each class, along with one standard deviation above and below. Since every trajectory using the histogram intensity estimator is piece-wise constant, so are the resulting PCA averages. The pairs of trajectories merge and split in a similar way to those obtained using the kernel smoother.

In Figures 5 and 6 show the first two spherical coordinates [44] of the trajectories obtained using the histogram intensity estimator and the Epanechnikov kernel smoother, respectively. The six plots correspond to the morning, lunchtime and afternoon across both days.

Figure 8 shows t-SNE visualisations of the node representations at a collection of times throughout the study. The plots are very similar to the equivalent Figure 4 for the kernel smoother with almost identical clusters of students before and after lunch, albeit placed differently by the t-SNE algorithm.

C Visualisation

In this section we give a short overview of the two dimension reduction techniques employed for visualisation in this paper.

For the trajectory visualisation in Figures 2 and 3, we use a principal component analysis which we extend to the dynamic setting by computing a projection using the leading eigenvectors of the *average* covariance matrix, which we apply to apply to the (globally centered) trajectories. This has a similar flavour to our Intensity Profile Projection algorithm, and since we reduce dimension using a common projection, it gives a temporally coherent view of the trajectories.

The second visualisation technique we apply is t-SNE [45], using the Flt-SNE implementation [46], apply we used to obtain Figure 4. This visualisation method is not naturally extended to dynamic data, so we initialise the algorithm using the aforementioned dynamic extension PCA, which results in the visualisations at different times being approximately aligned.

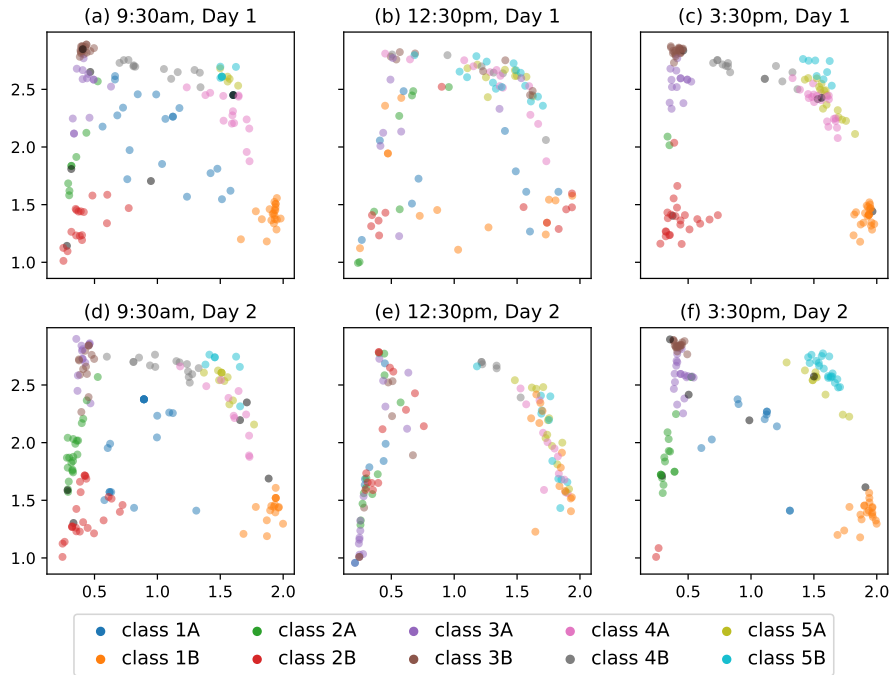


Figure 5: First two dimensions of the spherical coordinates of the coordinates $\widehat{X}_i(t)$ using the histogram intensity estimator for times corresponding to the morning, lunchtime and afternoon across both days. The colours indicate different classes with black points representing teachers.

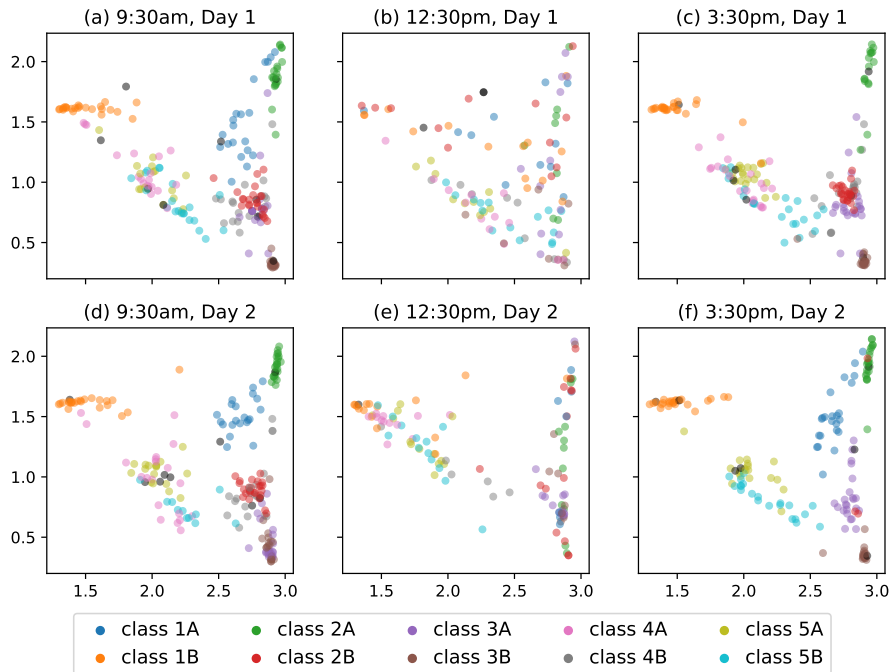


Figure 6: First two dimensions of the spherical coordinates of the trajectories $\widehat{X}_i(t)$ using the Epanechnikov kernel smoother for times corresponding to the morning, lunchtime and afternoon across both days. The colours indicate different classes with black points representing teachers.

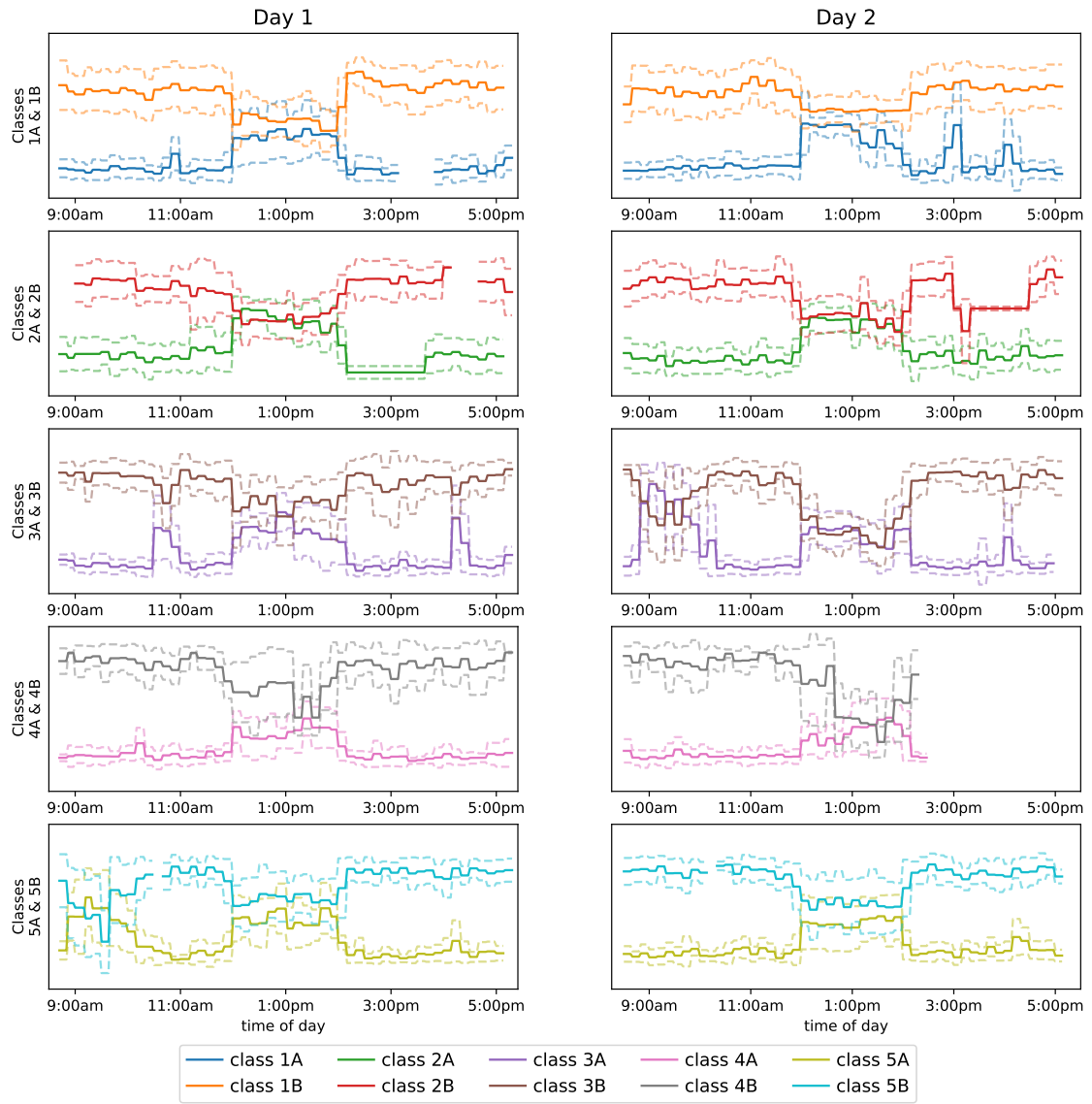


Figure 7: One-dimensional PCA visualisation of the 30-dimensional node representations for pairs of classes in the same year group. The solid lines show the average trajectory for each class, and the dashed line show one standard deviation above and below.

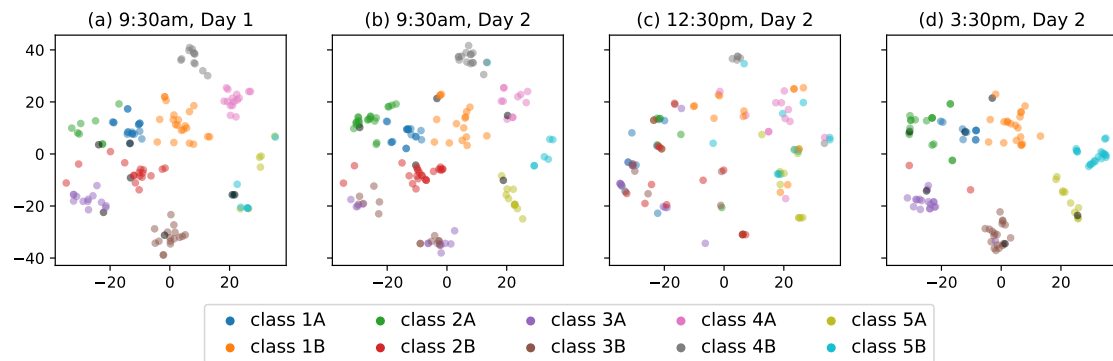


Figure 8: Two-dimensional t-SNE visualisation of the 30-dimensional node representations of all pupils and teachers evaluated at 9:30am on Day 1, and 9:30am, 12:30pm and 3:30pm on Day 2.

D Proof of Lemma 1

We begin by writing

$$\begin{aligned}
\arg \min_{\mathbf{V} \in \mathbb{O}(n,d)} R^2(\mathbf{V}) &= \arg \min_{\mathbf{V} \in \mathbb{O}(n,d)} R^2(\mathbf{V}) \int_0^T r_i^2(t; \mathbf{V}) dt \\
&= \arg \min_{\mathbf{V} \in \mathbb{O}(n,d)} \int_0^T \sum_{i=1}^n \left\| \mathbf{V} \mathbf{V}^\top \widehat{\Lambda}_i(t) - \widehat{\Lambda}_i(t) \right\|_2^2 dt \\
&= \arg \min_{\mathbf{V} \in \mathbb{O}(n,d)} \int_0^T \sum_{i=1}^n \left\| (\mathbf{I} - \mathbf{V} \mathbf{V}^\top) \widehat{\Lambda}_i(t) \right\|_2^2 dt,
\end{aligned}$$

and since $(\mathbf{I} - \mathbf{V} \mathbf{V}^\top)$ is the projection onto the orthogonal complement of the columns space of \mathbf{V} , we have that

$$\left\| \widehat{\Lambda}_i(t) \right\|_2^2 = \left\| \mathbf{V} \mathbf{V}^\top \widehat{\Lambda}_i(t) \right\|_2^2 + \left\| (\mathbf{I} - \mathbf{V} \mathbf{V}^\top) \widehat{\Lambda}_i(t) \right\|_2^2.$$

Therefore, minimising $R^2(\mathbf{V})$ is equivalent to maximising

$$\int_0^T \sum_{i=1}^n \left\| \mathbf{V} \mathbf{V}^\top \widehat{\Lambda}_i(t) \right\|_2^2 dt = \int_0^T \sum_{i=1}^n \left\| \mathbf{V}^\top \widehat{\Lambda}_i(t) \right\|_2^2 dt$$

where the equality holds due to the invariance of the Euclidean norm under orthogonal transformations. As a result, we have

$$\begin{aligned}
\arg \min_{\mathbf{V} \in \mathbb{O}(n,d)} R^2(\mathbf{V}) &= \arg \max_{\mathbf{V} \in \mathbb{O}(n,d)} \int_0^T \sum_{i=1}^n \left\| \mathbf{V}^\top \widehat{\Lambda}_i(t) \right\|_2^2 dt \\
&= \arg \max_{\mathbf{V} \in \mathbb{O}(n,d)} \int_0^T \left\| \widehat{\Lambda}(t) \mathbf{V} \right\|_F^2 dt \\
&= \arg \max_{\mathbf{V} \in \mathbb{O}(n,d)} \int_0^T \text{tr} \left\{ \mathbf{V}^\top \widehat{\Lambda}^2(t) \mathbf{V} \right\} dt \\
&= \arg \max_{\mathbf{V} \in \mathbb{O}(n,d)} \text{tr} \left\{ \mathbf{V}^\top \left(\int_0^T \widehat{\Lambda}^2(t) dt \right) \mathbf{V} \right\} \\
&= \arg \max_{\mathbf{V} \in \mathbb{O}(n,d)} \text{tr} \left\{ \mathbf{V}^\top \widehat{\Sigma} \mathbf{V} \right\} \\
&= \widehat{\mathbf{U}}
\end{aligned}$$

where the final equality follows from the Courant-Fisher min-max theorem. This concludes the proof.

E Proof of Theorem 1

E.1 Notation

In addition to the notation defined in the main text, we introduce the shorthand $a \stackrel{\mathbb{P}}{\lesssim} b$ to mean that $a \lesssim b$ with overwhelming probability.

E.2 Prerequisites

E.2.1 Symmetric dilation with change of basis “trick”

Symmetric dilation is a proof technique which allows statements about the eigenvectors of a symmetric matrix to be easily extended to hold for the singular vectors of a (potentially rectangular)

asymmetric matrix. Let \mathbf{M} be an $n_1 \times n_2$ matrix with non-zero singular values $\{\sigma_i\}_{i=1}^r$ and corresponding orthonormal left singular vectors $\{u_i\}_{i=1}^r$ and right singular vectors $\{v_i\}_{i=1}^r$. Its *symmetric dilation* is the $n \times n$ matrix (with $n = n_1 + n_2$) constructed as

$$\mathcal{D}(\mathbf{M}) = \begin{pmatrix} \mathbf{0} & \mathbf{M} \\ \mathbf{M}^\top & \mathbf{0} \end{pmatrix}.$$

One can easily verify that $\mathcal{D}(\mathbf{M})$ has eigenvalues $\{\pm\sigma_i\}_{i=1}^r$ and eigenvectors $\{(u_i^\top, \pm v_i^\top)^\top\}_{i=1}^r$. We stack the first d left and right singular vectors into matrices $\mathbf{U} \in \mathbb{R}^{n_1 \times d}$ and $\mathbf{V} \in \mathbb{R}^{n_2 \times d}$, and stack the first $2d$ eigenvectors of $\mathcal{D}(\mathbf{M})$ into a matrix

$$\bar{\mathbf{U}} = \frac{1}{\sqrt{2}} \begin{pmatrix} \mathbf{U} & \mathbf{U} \\ \mathbf{V} & -\mathbf{V} \end{pmatrix}.$$

We then have

$$\|\mathbf{U}\|_{2,\infty} \vee \|\mathbf{V}\|_{2,\infty} = \|\bar{\mathbf{U}}\|_{2,\infty}, \quad \text{and} \quad \|\mathbf{M}\|_2 = \|\mathcal{D}(\mathbf{M})\|_2.$$

While this standard construction is very useful when $n_1 \asymp n_2$, it can lead to suboptimal bounds when $n_2 \gg n_1$, or $n_1 \gg n_2$, due to an issue about incoherence, which was first raised in [47]. The *incoherence* of a subspace \mathcal{U}_0 spanned by the orthonormal columns of a matrix $\mathbf{U}_0 \in \mathbb{R}^{n_0 \times d}$ is

$$\mu(\mathbf{U}_0) = \sqrt{\frac{n_0}{d}} \|\mathbf{U}_0\|_{2,\infty}.$$

To obtain a good bound on $\|\bar{\mathbf{U}}\|_{2,\infty}$ it is typically necessary that $\mu(\bar{\mathbf{U}}) \asymp 1$. Observe that

$$\mu(\bar{\mathbf{U}}) = \sqrt{\frac{n_1 + n_2}{2d}} \|\bar{\mathbf{U}}\|_{2,\infty} = \sqrt{\frac{n_1 + n_2}{2d}} \left(\|\mathbf{U}\|_{2,\infty} \vee \|\mathbf{V}\|_{2,\infty} \right) = \sqrt{\frac{n_1 + n_2}{2n_1}} \mu(\mathbf{U}) + \sqrt{\frac{n_1 + n_2}{2n_2}} \mu(\mathbf{V}).$$

If $\mu(\mathbf{U}), \mu(\mathbf{V}) \asymp 1$ and $n_1 \asymp n_2$, then $\mu(\bar{\mathbf{U}}) \asymp 1$ and it is typically possible to obtain good bounds. However, when $n_2 \gg n_1$, we have $\mu(\bar{\mathbf{U}}) \gg 1$, and a good bound can typically not be obtained. The imbalance of n_1 and n_2 can cause similar issues when obtaining spectral norm bounds.

This issue can be overcome by bounding $\bar{\mathbf{U}}$ with respect to a basis which balances the contribution from its first n_1 and second n_2 elements of each column. Specifically, let $\pi_1 = \sqrt{2n_1/(n_1 + n_2)}$ and $\pi_2 = \sqrt{2n_2/(n_1 + n_2)}$, and consider the basis $\tilde{e}_1, \dots, \tilde{e}_{n_1+n_2}$, such that

$$e_i = \begin{cases} \pi_1 \tilde{e}_i & \text{if } i \in \{1, \dots, n_1\} \\ \pi_2 \tilde{e}_i & \text{if } i \in \{n_1 + 1, \dots, n_1 + n_2\}, \end{cases}$$

where $\{e_i\}_{i=1}^{n_1+n_2}$ are the standard basis vectors in \mathbb{R}^{n_0} . Let $\|\cdot\|$ denote a generic norm with respect to the column basis $\{\tilde{e}_i\}_{i=1}^{n_1+n_2}$, then one can verify that

$$\|\mathcal{D}(\mathbf{M})\|_2 = \|\mathbf{M}\|, \quad \text{and} \quad \|\bar{\mathbf{U}}\|_{2,\infty} = \pi_1 \|\mathbf{U}\|_{2,\infty} \vee \pi_2 \|\mathbf{V}\|_{2,\infty}.$$

As a result, if $\tilde{\mu}(\mathbf{U}_0) = \sqrt{n_0/d} \|\mathbf{U}_0\|_{2,\infty}$, then

$$\tilde{\mu}(\bar{\mathbf{U}}) = \mu(\mathbf{U}) \vee \mu(\mathbf{V}),$$

regardless of the relative sizes of n_1 and n_2 . We use this symmetric dilation with change of basis “trick” to apply some existing theorems for symmetric matrices to our setting.

E.2.2 Concentration inequalities

In this section, we state a collection of lemmas which we will make use of throughout the proof. We begin with a tail bound for a Poisson random variable.

Lemma 3. *Let $X \sim \text{Poisson}(\lambda)$. Then*

$$\mathbb{P}(|X - \lambda| \geq t) \leq 2 \exp\left(-\frac{t^2}{2(\lambda + t/3)}\right).$$

For $t \geq \lambda$,

$$\mathbb{P}(|X - \lambda| \geq t) \leq 2e^{-3t/8}.$$

The bound can be established by approximating the Poisson distribution with mean λ as the sum of k Bernoulli random variables with mean λ/k , applying Bernstein's inequality, and taking $k \rightarrow 0$.

Our next result is a concentration bound which adapts Lemma A.1 of [15] and can be proved using a vector version of the Bernstein inequality (Corollary 4.1 in [48]).

Lemma 4. *Let $X_i \sim \text{Poisson}(\lambda_i)$ independently for all $i = 1, \dots, n$, and suppose $\mathbf{Q} \in \mathbb{R}^{n \times d}$ is a deterministic matrix whose rows we denote Q_i . Let $\lambda_{\max} := \max_{i \in [n]} \lambda_i$, then with probability $1 - 28n^{-3}$*

$$\left\| \sum_{i=1}^n (X_i - \lambda_i) Q_i \right\|_2 \leq 3 \log^2 n \|\mathbf{Q}\|_{2, \infty} + \sqrt{6 \lambda_{\max} \log n} \|\mathbf{Q}\|_F.$$

Next, we state a concentration bound for the spectral norm of random matrices with independent entries which appears as Corollary 3.12 in [49]. The original statement of this lemma is for symmetric random matrices, although we general it to arbitrary random matrices using the symmetric dilation with change of basis trick described in Section E.2.1.

Lemma 5 (Corollary 3.12 of [49]). *Let \mathbf{X} be an $n_1 \times n_2$ matrix whose entries x_{ij} are independent random variables which obey*

$$\mathbb{E}(x_{ij}) = 0, \quad \text{and} \quad |x_{ij}| \leq B, \quad i \in [n_1], j \in [n_2].$$

Then there exists a universal constant $c > 0$ such that for any $t \geq 0$

$$\mathbb{P}\{\|\mathbf{X}\| \geq 4\sqrt{\nu} + t\} \leq n \exp\left(-\frac{t^2}{cB^2}\right).$$

where

$$\nu := \max \left\{ \pi_1 \max_{i \in [n_1]} \sum_{j=1}^{n_2} \mathbb{E}(x_{ij}^2), \pi_2 \max_{i \in [n_2]} \sum_{j=1}^{n_1} \mathbb{E}(x_{ji}^2) \right\}$$

and $\pi_k = 2n_k/(n_1 + n_2)$.

E.2.3 Weyl's inequality and Wedin's $\sin\Theta$ theorem

The next two lemmas are classical results matrix perturbation theory. Weyl's inequality shows that the singular values of a matrix are stable with respect to small perturbations.

Lemma 6 (Weyl's inequality). *Let \mathbf{M}, \mathbf{E} be $n_1 \times n_2$ real-valued matrices. Then for every $1 \leq i \leq (n_1 \wedge n_2)$, the i th largest singular value of \mathbf{M} and $\mathbf{M} + \mathbf{E}$ obey*

$$|\sigma_i(\mathbf{M} + \mathbf{E}) - \sigma_i(\mathbf{M})| \leq \|\mathbf{E}\|_2.$$

One way to measure the distance between two subspaces \mathcal{U} and $\widehat{\mathcal{U}}$ is via principal angles. Let $\mathbf{U}, \widehat{\mathbf{U}}$ be matrices whose orthonormal columns span \mathcal{U} and $\widehat{\mathcal{U}}$ respectively, and let $\{\xi_i\}_{i=1}^d$ denote the singular values of $\mathbf{U}^\top \widehat{\mathbf{U}}$. Then the principal angles $\{\theta_i\}_{i=1}^d$ between \mathcal{U} and $\widehat{\mathcal{U}}$ are defined by $\xi_i = \cos(\theta_i)$. Let $\sin \Theta(\mathbf{U}, \widehat{\mathbf{U}}) := \text{diag}(\sin \theta_1, \dots, \sin \theta_d)$. Another way to measure the distance between \mathcal{U} and $\widehat{\mathcal{U}}$ is via the difference between the projection operators $\mathbf{U}\mathbf{U}^\top$ and $\widehat{\mathbf{U}}\widehat{\mathbf{U}}^\top$, and in fact, these two characterisations are equivalent. Specifically,

$$\left\| \sin \Theta(\mathbf{U}, \widehat{\mathbf{U}}) \right\|_2 \equiv \left\| \mathbf{U}\mathbf{U}^\top - \widehat{\mathbf{U}}\widehat{\mathbf{U}}^\top \right\|_2.$$

We will use this equivalence without mention throughout the proof. Wedin's $\sin\Theta$ theorem shows that the singular vectors of a matrix are stable with respect to small perturbations.

Lemma 7. *Let \mathbf{M} and $\widehat{\mathbf{M}} = \mathbf{M} + \mathbf{E}$ be two $n_1 \times n_2$ real-valued matrices, and denote by $\mathbf{U}, \widehat{\mathbf{U}}$ (respectively $\mathbf{V}, \widehat{\mathbf{V}}$) the matrices whose columns contain d orthonormal left (respectively, right) singular vectors, corresponding to the d largest singular values of \mathbf{M} and $\widehat{\mathbf{M}}$. Let $\delta = \sigma_d(\mathbf{M}) - \sigma_{d+1}(\mathbf{M})$ and suppose that $\|\mathbf{E}\| < (1 - 1/\sqrt{2})\delta$, then*

$$\left\| \sin\Theta(\mathbf{U}, \widehat{\mathbf{U}}) \right\|_2 \leq \frac{2(\|\mathbf{E}^\top \mathbf{U}\|_2 \vee \|\mathbf{E}\mathbf{V}\|_2)}{\delta} \leq \frac{2\|\mathbf{E}\|}{\delta}.$$

See [50] for a proof.

E.3 Implications of Assumptions 1-4

We state here some inequalities involving the parameters of our problem which follow from Assumptions 1-4, and elementary linear algebra. We will use these facts throughout the proof without mention.

$$\sqrt{n\lambda_{\max}} \ll \delta \leq n\lambda_{\max}; \quad (4)$$

$$\delta \log n \gtrsim \kappa n\lambda_{\max}; \quad (5)$$

$$\kappa \lesssim \log n. \quad (6)$$

The inequality (4) holds since $\delta \leq \sigma_1^{1/2}(\boldsymbol{\Sigma}) \leq \sqrt{n}\|\boldsymbol{\Sigma}\|_{\max}^{1/2} \leq n\lambda_{\max}$, and

$$\delta \gtrsim \frac{\kappa n\lambda_{\max}}{\log(\delta/\sqrt{n\lambda_{\max}})} \gtrsim \frac{n\lambda_{\max}}{\log n} \gg \sqrt{n\lambda_{\max} \log n} \gtrsim \sqrt{n\lambda_{\max}}$$

where we invoked Assumption 4. (5) holds by noting that the previous bound implies $\log(\delta/\sqrt{n\lambda_{\max}}) \lesssim \log n$ and invoking Assumption 2. (6) follows from (4) since $\kappa \lesssim \delta \log n / n\lambda_{\max} \lesssim \log n$.

E.4 Setup

We begin by defining M equally spaced bins in $(0, 1]$,

$$B_1 := \left(0, \frac{1}{M}\right], \quad B_2 := \left(\frac{1}{M}, \frac{2}{M}\right], \dots, \quad B_M := \left(\frac{M-1}{M}, 1\right],$$

and define the piecewise approximation of $\lambda_i(t)$,

$$\bar{\lambda}_i(t) = M \int_{B_m} \lambda_i(t) dt, \quad t \in B_m, \quad m \in [M].$$

We then define $t_1, \dots, t_m \in (0, 1]$ such that $\bar{\lambda}_{ij}(t) = \lambda_{ij}(t_m)$ for all $t \in B_m$, which exist by the continuity of $\lambda_{ij}(t)$, and define the piecewise constant approximation of $Y_i(t)$ as $\bar{Y}_i(t) = \mathbf{U}^\top \Lambda_i(t)$. Our strategy to obtain the bound in Theorem 1 is to decompose it into bias and variance terms

$$\max_{i,j \in [n]} \sup_{t \in \mathcal{T}} \left\| \mathbf{W}_1 \widehat{Y}_i(t) - Y_i(t) \right\|_2 = \underbrace{\max_{i,j \in [n]} \sup_{t \in \mathcal{T}} \left\| \mathbf{W}_1 \widehat{Y}_i(t) - \bar{Y}_i(t) \right\|_2}_{\text{variance}} + \underbrace{\max_{i,j \in [n]} \sup_{t \in \mathcal{T}} \left\| \mathbf{W}_2 \bar{Y}_i(t) - Y_i(t) \right\|_2}_{\text{bias}}.$$

Section E.7 is dedicated to bounding the bias term, and the rest of this section is dedicated to bounding the variance term. Define the unfolding matrices $\widehat{\boldsymbol{\Lambda}}$ and $\boldsymbol{\Lambda}$ (without arguments) and their (thin) singular value decompositions as

$$\begin{aligned} \widehat{\boldsymbol{\Lambda}} &:= \left(\widehat{\boldsymbol{\Lambda}}(t_1) \cdots \widehat{\boldsymbol{\Lambda}}(t_M) \right) = \widehat{\mathbf{U}} \widehat{\boldsymbol{\Sigma}} \widehat{\mathbf{V}}^\top + \widehat{\mathbf{U}}_\perp \widehat{\boldsymbol{\Sigma}}_\perp \widehat{\mathbf{V}}_\perp^\top, \\ \bar{\boldsymbol{\Lambda}} &:= (\boldsymbol{\Lambda}(t_1) \cdots \boldsymbol{\Lambda}(t_M)) = \bar{\mathbf{U}} \bar{\boldsymbol{\Sigma}} \bar{\mathbf{V}}^\top + \bar{\mathbf{U}}_\perp \bar{\boldsymbol{\Sigma}}_\perp \bar{\mathbf{V}}_\perp^\top. \end{aligned}$$

Then one has that for $t \in B_m$, $m \in [M]$,

$$\widehat{\mathbf{Y}}(t) := \widehat{\mathbf{\Lambda}}(t_m)\widehat{\mathbf{U}} = \widehat{\mathbf{V}}_m\widehat{\mathbf{S}}, \quad \bar{\mathbf{Y}}(t) := \bar{\mathbf{\Lambda}}(t_m)\bar{\mathbf{U}} = \bar{\mathbf{V}}_m\bar{\mathbf{S}}$$

where $\widehat{\mathbf{V}}_m, \bar{\mathbf{V}}_m$ denote the m th blocks of $\widehat{\mathbf{V}}$ and $\bar{\mathbf{V}}$ respectively. Therefore it follows that,

$$\max_{i,j \in [n]} \sup_{t \in \mathcal{T}} \left\| \mathbf{W}_1 \widehat{Y}_i(t) - \bar{Y}_i(t) \right\|_2 = \left\| \widehat{\mathbf{V}}\widehat{\mathbf{S}}\mathbf{W}_1^\top - \bar{\mathbf{V}}\bar{\mathbf{S}} \right\|_{2,\infty}.$$

For ease of exposition, we drop the subscript 1 on \mathbf{W}_1 in this section. Our bound is based on the following decomposition of $\widehat{\mathbf{V}}\widehat{\mathbf{S}} - \bar{\mathbf{V}}\bar{\mathbf{S}}\mathbf{W}$.

Proposition 1. *We have the decomposition*

$$\widehat{\mathbf{V}}\widehat{\mathbf{S}} - \bar{\mathbf{V}}\bar{\mathbf{S}}\mathbf{W} = \bar{\mathbf{V}}(\bar{\mathbf{V}}^\top \widehat{\mathbf{V}}\widehat{\mathbf{S}} - \bar{\mathbf{S}}\mathbf{W}) \tag{7}$$

$$+ (\mathbf{I} - \bar{\mathbf{V}}\bar{\mathbf{V}}^\top)\bar{\mathbf{\Lambda}}^\top \tag{8}$$

$$+ (\mathbf{I} - \bar{\mathbf{V}}\bar{\mathbf{V}}^\top)(\widehat{\mathbf{\Lambda}} - \bar{\mathbf{\Lambda}})^\top \bar{\mathbf{U}}\mathbf{W} \tag{9}$$

$$+ (\mathbf{I} - \bar{\mathbf{V}}\bar{\mathbf{V}}^\top)(\widehat{\mathbf{\Lambda}} - \bar{\mathbf{\Lambda}})^\top (\widehat{\mathbf{U}} - \bar{\mathbf{U}}\mathbf{W}). \tag{10}$$

Proof of Proposition 1. We begin by adding and subtracting terms to obtain

$$\widehat{\mathbf{V}}\widehat{\mathbf{S}} - \bar{\mathbf{V}}\bar{\mathbf{S}}\mathbf{W} = \widehat{\mathbf{V}}\widehat{\mathbf{S}} - \bar{\mathbf{V}}\bar{\mathbf{V}}^\top \widehat{\mathbf{V}}\widehat{\mathbf{S}} + \underbrace{\bar{\mathbf{V}}(\bar{\mathbf{V}}^\top \widehat{\mathbf{V}}\widehat{\mathbf{S}} - \bar{\mathbf{S}}\mathbf{W})}_{(7)}.$$

Then, noting that $\widehat{\mathbf{V}}\widehat{\mathbf{S}} = \widehat{\mathbf{\Lambda}}^\top \widehat{\mathbf{U}}$ and $\bar{\mathbf{V}}\bar{\mathbf{V}}^\top \bar{\mathbf{\Lambda}}^\top = \bar{\mathbf{\Lambda}}^\top - (\mathbf{I} - \bar{\mathbf{V}}\bar{\mathbf{V}}^\top)\bar{\mathbf{\Lambda}}^\top$, we have

$$\begin{aligned} \widehat{\mathbf{V}}\widehat{\mathbf{S}} - \bar{\mathbf{V}}\bar{\mathbf{V}}^\top \widehat{\mathbf{V}}\widehat{\mathbf{S}} &= \widehat{\mathbf{\Lambda}}^\top \widehat{\mathbf{U}} - \bar{\mathbf{V}}\bar{\mathbf{V}}^\top \widehat{\mathbf{\Lambda}}^\top \widehat{\mathbf{U}} \\ &= (\widehat{\mathbf{\Lambda}} - \bar{\mathbf{\Lambda}})^\top \widehat{\mathbf{U}} - (\bar{\mathbf{V}}\bar{\mathbf{V}}^\top \widehat{\mathbf{\Lambda}}^\top - \bar{\mathbf{\Lambda}}^\top) \widehat{\mathbf{U}} \\ &= (\mathbf{I} - \bar{\mathbf{V}}\bar{\mathbf{V}}^\top)(\widehat{\mathbf{\Lambda}} - \bar{\mathbf{\Lambda}})^\top \widehat{\mathbf{U}} - \underbrace{(\mathbf{I} - \bar{\mathbf{V}}\bar{\mathbf{V}}^\top)\bar{\mathbf{\Lambda}}^\top}_{(8)}. \end{aligned}$$

Next, we decompose $(\mathbf{I} - \bar{\mathbf{V}}\bar{\mathbf{V}}^\top)(\widehat{\mathbf{\Lambda}} - \bar{\mathbf{\Lambda}})^\top \widehat{\mathbf{U}}$ by adding and subtracting terms to obtain

$$(\mathbf{I} - \bar{\mathbf{V}}\bar{\mathbf{V}}^\top)(\widehat{\mathbf{\Lambda}} - \bar{\mathbf{\Lambda}})^\top \widehat{\mathbf{U}} = \underbrace{(\mathbf{I} - \bar{\mathbf{V}}\bar{\mathbf{V}}^\top)(\widehat{\mathbf{\Lambda}} - \bar{\mathbf{\Lambda}})^\top \bar{\mathbf{U}}\mathbf{W}}_{(9)} + \underbrace{(\mathbf{I} - \bar{\mathbf{V}}\bar{\mathbf{V}}^\top)(\widehat{\mathbf{\Lambda}} - \bar{\mathbf{\Lambda}})^\top (\widehat{\mathbf{U}} - \bar{\mathbf{U}}\mathbf{W})}_{(10)}.$$

□

E.5 Technical propositions

We now outline a series of technical propositions which we require to bound terms (7)-(10) which we prove in Section F.

Our first proposition is a 1-norm and spectral norm bound for $\widehat{\mathbf{\Lambda}}$.

Proposition 2. *The bounds*

$$\left\| \widehat{\mathbf{\Lambda}} - \bar{\mathbf{\Lambda}} \right\|_1 \lesssim \sqrt{Mn\lambda_{\max} \log n}, \quad \left\| \widehat{\mathbf{\Lambda}} - \bar{\mathbf{\Lambda}} \right\|_2 \lesssim \sqrt{Mn\lambda_{\max}}$$

hold with overwhelming probability.

The spectral norm bound is obtained using Lemma 5, and the 1-norm bound is obtained via an application of the classical Bernstein inequality. The next proposition provides control on the singular values of $\widehat{\mathbf{\Lambda}}$.

Proposition 3. Let $\sigma_i(\cdot)$ denote the i th ordered singular value of a matrix. The singular values of $\widehat{\Lambda}$ satisfy

$$\sqrt{M\sigma_d(\Sigma)} \lesssim \sigma_d(\widehat{\Lambda}) \leq \sigma_1(\widehat{\Lambda}) \lesssim \sqrt{M\sigma_1(\Sigma)}.$$

The result is obtained using Weyl's inequality. The next proposition provides control of the spectral norm of $\mathbf{Q}^\top(\widehat{\Lambda} - \bar{\Lambda})\mathbf{R}$, where \mathbf{Q}, \mathbf{R} are conformable, deterministic unit-norm matrices.

Proposition 4. For conformable, deterministic unit-norm matrices \mathbf{Q}, \mathbf{R} , the bound

$$\left\| \mathbf{Q}^\top(\widehat{\Lambda} - \bar{\Lambda})\mathbf{R} \right\|_2 \lesssim M \log^{3/2} n \quad (11)$$

holds with overwhelming probability.

The proof of Proposition 4 employs a classical ε -net argument to the spectral norm of an appropriately constructed symmetric dilation matrix.

The next proposition states that both the matrices $\bar{\mathbf{U}}^\top \widehat{\mathbf{U}}$ and $\bar{\mathbf{V}}^\top \widehat{\mathbf{V}}$ are well approximated by a common orthogonal matrix.

Proposition 5. There exists an orthogonal matrix \mathbf{W} such that

$$\left\| \bar{\mathbf{U}}^\top \widehat{\mathbf{U}} - \mathbf{W} \right\|_2 \lesssim \frac{\sqrt{n\lambda_{\max}}}{\delta}, \quad \left\| \bar{\mathbf{V}}^\top \widehat{\mathbf{V}} - \mathbf{W} \right\|_2 \lesssim \frac{\sqrt{n\lambda_{\max}}}{\delta}$$

hold with overwhelming probability.

To prove Proposition 5, we employ the Wedin $\sin\Theta$ theorem to obtain a bound on $\|\bar{\mathbf{U}}^\top \widehat{\mathbf{U}} - \mathbf{W}\|_2$. We then obtain a bound on $\|\bar{\mathbf{U}}^\top \widehat{\mathbf{U}} - \bar{\mathbf{V}}^\top \widehat{\mathbf{V}}\|_2$, and combine these bound to establish the proposition.

The next technical tool we require is the ability to “swap” $\mathbf{W}, \bar{\mathbf{S}}$ and $\widehat{\mathbf{S}}$.

Proposition 6. The bound

$$\left\| \mathbf{W}\widehat{\mathbf{S}} - \bar{\mathbf{S}}\mathbf{W} \right\|_2 \lesssim M \log^{3/2} n$$

holds with overwhelming probability.

This result follows by applying the previous propositions to an appropriately constructed decomposition.

Part of the challenge of obtaining a good bound on the term (10) is that $(\tilde{\mathbf{A}} - \tilde{\Lambda})$ and $(\widehat{\mathbf{U}} - \bar{\mathbf{U}}\mathbf{W})$ are dependent, and this dependence must be decoupled in order to apply the standard suite of matrix perturbation tools. For $m = 1, \dots, n$, let

$$\mathcal{N}_m = \{(i, j) : i = m \text{ or } j \in \{m + (\ell - 1)n, \ell \in [M]\}\}$$

and construct the auxiliary matrices $\widehat{\Lambda}^{(1)}, \dots, \widehat{\Lambda}^{(n)}$ defined by

$$\widehat{\Lambda}_{ij}^{(m)} = \begin{cases} \widehat{\Lambda}_{ij} & \text{if } (i, j) \notin \mathcal{N}_m, \\ \bar{\Lambda}_{ij} & \text{if } (i, j) \in \mathcal{N}_m. \end{cases}$$

In words, $\widehat{\Lambda}_{ij}^{(m)}$ is the matrix obtained by replacing the m th row and columns of each of its blocks with its expectation. In this way, the m th row of $(\widehat{\Lambda} - \bar{\Lambda})$ and $\widehat{\Lambda}^{(m)}$ are independent. Let $\widehat{\mathbf{U}}^{(m)}$ denote the matrix of leading left singular values of $\widehat{\Lambda}^{(m)}$.

We apply a result due to [13], which provides $\ell_{2,\infty}$ control of $\|\widehat{\mathbf{U}}\|_{2,\infty}$, $\|\widehat{\mathbf{U}}^{(m)}\|_{2,\infty}$, and $\|\widehat{\mathbf{U}}^{(m)}\mathbf{W}^{(m)} - \mathbf{U}\|_{2,\infty}$.

Proposition 7. *The bounds*

$$\left\| \widehat{\mathbf{U}} \right\|_{2,\infty}, \left\| \widehat{\mathbf{U}}^{(m)} \right\|_{2,\infty}, \left\| \widehat{\mathbf{U}}^{(m)} \mathbf{W}^{(m)} - \mathbf{U} \right\|_{2,\infty} \lesssim \frac{\mu \lambda_{\max} \sqrt{dn} \log n}{\delta}$$

hold with overwhelming probability.

In addition, we require control on the spectral norm difference between the projection matrices $\widehat{\mathbf{U}}^{(m)}(\widehat{\mathbf{U}}^{(m)})^\top$ and the projection matrices $\bar{\mathbf{U}}\bar{\mathbf{U}}^\top$ and $\widehat{\mathbf{U}}\widehat{\mathbf{U}}^\top$, which is provided in the following proposition.

Proposition 8. *The bounds*

$$\left\| \widehat{\mathbf{U}}^{(m)}(\widehat{\mathbf{U}}^{(m)})^\top - \bar{\mathbf{U}}\bar{\mathbf{U}}^\top \right\|_2 \lesssim \frac{n\lambda_{\max}}{\delta}, \quad (12)$$

$$\left\| \widehat{\mathbf{U}}^{(m)}(\widehat{\mathbf{U}}^{(m)})^\top - \widehat{\mathbf{U}}\widehat{\mathbf{U}}^\top \right\|_2 \lesssim \frac{\mu \lambda_{\max}^{3/2} \sqrt{dn} \log^{3/2} n}{\delta^2} \quad (13)$$

hold with overwhelming probability.

The proof of Proposition 8 requires a delicate “leave-one-out”-style argument.

E.6 Bounding terms (7)-(10)

Firstly observe that

$$\left\| \bar{\mathbf{V}} \right\|_{2,\infty} = \left\| \bar{\mathbf{A}}^\top \bar{\mathbf{U}} \bar{\mathbf{S}}^{-1} \right\|_{2,\infty} \leq \left\| \bar{\mathbf{A}}^\top \right\|_\infty \left\| \bar{\mathbf{U}} \right\|_{2,\infty} \left\| \bar{\mathbf{S}}^{-1} \right\|_2 \leq \frac{\sqrt{nd} \lambda_{\max} \mu}{\sqrt{M \sigma_d(\boldsymbol{\Sigma})}}$$

and therefore term (7) can be bounded as

$$\begin{aligned} \left\| \bar{\mathbf{V}}(\bar{\mathbf{V}}^\top \widehat{\mathbf{V}} \widehat{\mathbf{S}} - \bar{\mathbf{S}} \mathbf{W}) \right\|_{2,\infty} &\leq \left\| \bar{\mathbf{V}} \right\|_{2,\infty} \left(\left\| \bar{\mathbf{V}}^\top \widehat{\mathbf{V}} - \mathbf{W} \right\|_2 \left\| \widehat{\mathbf{S}} \right\| + \left\| \mathbf{W} \widehat{\mathbf{S}} - \bar{\mathbf{S}} \mathbf{W} \right\|_2 \right) \\ &\stackrel{\mathbb{P}}{\lesssim} \frac{\sqrt{nd} \lambda_{\max} \mu}{\sqrt{M \sigma_d(\boldsymbol{\Sigma})}} \left(\frac{\sqrt{n \lambda_{\max}}}{\delta} \cdot \sqrt{M \sigma_1(\boldsymbol{\Sigma})} + M \log^{3/2} n \right) \\ &\lesssim \frac{n \sqrt{M d} \lambda_{\max}^{3/2} \mu \kappa}{\delta} \\ &\lesssim \mu \sqrt{M \lambda_{\max} d} \log n. \end{aligned}$$

where the third inequality follows from Assumption 4 that $\sqrt{M} \log^{3/2} n \lesssim n \lambda_{\max}$, and the definition $\kappa := \sqrt{\sigma_1(\boldsymbol{\Sigma})/\sigma_d(\boldsymbol{\Sigma})}$, and the fourth inequality follows from Assumption 2 that $\delta \log n \geq \delta \log(\delta/\sqrt{n \lambda_{\max}}) \gtrsim \kappa n \lambda_{\max}$.

Term (8) can be bounded deterministically using Assumption 3 as

$$\left\| (\mathbf{I} - \bar{\mathbf{V}} \bar{\mathbf{V}}^\top) \bar{\mathbf{A}}^\top \right\|_{2,\infty} = \left\| \bar{\mathbf{A}}^\top (\mathbf{I} - \bar{\mathbf{U}} \bar{\mathbf{U}}) \right\|_{2,\infty} \lesssim \max_{i \in [n]} \sup_{t \in \mathcal{T}} r_i(t) \lesssim \mu \sqrt{d \lambda_{\max}} \log^{5/2} n.$$

To bound term (9), we set $\mathbf{E} = \widehat{\mathbf{A}} - \bar{\mathbf{A}}$ and note that each column of $M^{-1} \mathbf{E}$ contains independent Poisson random variables with means no greater than $M^{-1} \lambda_{\max}$. We will use Lemma 4 to bound the rows $\mathbf{E} \bar{\mathbf{U}}$ as

$$\begin{aligned} [\mathbf{E}^\top \bar{\mathbf{U}}]_i &= \sum_{j=1}^n e_{ji} \bar{U}_j \stackrel{\mathbb{P}}{\lesssim} M \log^2 n \left\| \bar{\mathbf{U}} \right\|_{2,\infty} + \sqrt{M \lambda_{\max} \log n} \left\| \bar{\mathbf{U}} \right\|_{\text{F}} \\ &\lesssim \left(M \log^2 n + \sqrt{M n \lambda_{\max} \log n} \right) \left\| \bar{\mathbf{U}} \right\|_{2,\infty} \\ &\lesssim \sqrt{M \lambda_{\max} n \log n} \left\| \bar{\mathbf{U}} \right\|_{2,\infty} \\ &\lesssim \mu \sqrt{M \lambda_{\max} d} \log n. \end{aligned}$$

where the third inequality uses Assumption 4 and a union bound over $i = 1, \dots, n$. Therefore, we have

$$\|(\widehat{\mathbf{\Lambda}} - \bar{\mathbf{\Lambda}})^\top \bar{\mathbf{U}}\|_{2,\infty} \stackrel{\mathbb{P}}{\lesssim} \sqrt{M\lambda_{\max}d \log n}. \quad (14)$$

Noting that $\|\mathbf{I} - \bar{\mathbf{V}}\bar{\mathbf{V}}^\top\|_\infty \leq \|\mathbf{I} - \bar{\mathbf{V}}\bar{\mathbf{V}}^\top\|_2 \lesssim 1$, we bound (9) as

$$\|(\mathbf{I} - \bar{\mathbf{V}}\bar{\mathbf{V}}^\top)(\widehat{\mathbf{\Lambda}} - \bar{\mathbf{\Lambda}})^\top \bar{\mathbf{U}}\mathbf{W}\|_{2,\infty} \lesssim \|\mathbf{I} - \bar{\mathbf{V}}\bar{\mathbf{V}}^\top\|_\infty \left\| (\widehat{\mathbf{\Lambda}} - \bar{\mathbf{\Lambda}})^\top \bar{\mathbf{U}} \right\|_{2,\infty} \stackrel{\mathbb{P}}{\lesssim} \mu\sqrt{M\lambda_{\max}d \log n}.$$

Let $\widehat{\mathbf{\Lambda}}^{(1)}, \dots, \widehat{\mathbf{\Lambda}}^{(n)}$ denote the auxiliary matrices described in (E.5), and let $\widehat{\mathbf{U}}^{(m)}$ denote the matrix of leading left singular values of $\widehat{\mathbf{\Lambda}}^{(m)}$. We can then decompose the Euclidean norm of $(\widehat{\mathbf{\Lambda}} - \bar{\mathbf{\Lambda}})_{\cdot,m}^\top (\widehat{\mathbf{U}} - \mathbf{U}\mathbf{W})$ as

$$\left\| (\widehat{\mathbf{\Lambda}} - \bar{\mathbf{\Lambda}})_{\cdot,m}^\top (\widehat{\mathbf{U}} - \mathbf{U}\mathbf{W}) \right\|_2 \leq \left\| (\widehat{\mathbf{\Lambda}} - \bar{\mathbf{\Lambda}})_{\cdot,m}^\top \widehat{\mathbf{U}} (\mathbf{W} - \widehat{\mathbf{U}}^\top \bar{\mathbf{U}}) \right\|_2 \quad (15)$$

$$+ \left\| (\widehat{\mathbf{\Lambda}} - \bar{\mathbf{\Lambda}})_{\cdot,m}^\top (\widehat{\mathbf{U}}\widehat{\mathbf{U}}^\top \bar{\mathbf{U}} - \widehat{\mathbf{U}}^{(m)}(\widehat{\mathbf{U}}^{(m)})^\top \bar{\mathbf{U}}) \right\|_2 \quad (16)$$

$$+ \left\| (\widehat{\mathbf{\Lambda}} - \bar{\mathbf{\Lambda}})_{\cdot,m}^\top (\widehat{\mathbf{U}}^{(m)}(\widehat{\mathbf{U}}^{(m)})^\top \bar{\mathbf{U}} - \bar{\mathbf{U}}) \right\|_2. \quad (17)$$

The first term (15) is bounded as

$$\begin{aligned} \left\| (\widehat{\mathbf{\Lambda}} - \bar{\mathbf{\Lambda}})_{\cdot,m}^\top \widehat{\mathbf{U}} (\mathbf{W} - \widehat{\mathbf{U}}^\top \bar{\mathbf{U}}) \right\|_2 &\leq \left\| \widehat{\mathbf{\Lambda}} - \bar{\mathbf{\Lambda}} \right\|_1 \left\| \widehat{\mathbf{U}} \right\|_{2,\infty} \left\| \mathbf{W} - \widehat{\mathbf{U}}^\top \bar{\mathbf{U}} \right\|_2 \\ &\stackrel{\mathbb{P}}{\lesssim} \sqrt{Mn\lambda_{\max} \log n} \cdot \frac{\mu\lambda_{\max}\sqrt{dn} \log n}{\delta} \cdot \frac{\sqrt{n\lambda_{\max}}}{\delta} \\ &= \frac{\sqrt{M}n^{3/2}\lambda_{\max}^2\mu\sqrt{d} \log^{3/2} n}{\delta^2} \\ &\lesssim \mu\sqrt{M\lambda_{\max}d} \log^{5/2} n. \end{aligned}$$

To bound the second term (16), we employ Proposition 8 to obtain

$$\begin{aligned} \left\| (\widehat{\mathbf{\Lambda}} - \bar{\mathbf{\Lambda}})_{\cdot,m}^\top (\widehat{\mathbf{U}}\widehat{\mathbf{U}}^\top \bar{\mathbf{U}} - \widehat{\mathbf{U}}^{(m)}(\widehat{\mathbf{U}}^{(m)})^\top \bar{\mathbf{U}}) \right\|_2 &\leq \left\| \widehat{\mathbf{\Lambda}} - \bar{\mathbf{\Lambda}} \right\|_2 \left\| \widehat{\mathbf{U}}\widehat{\mathbf{U}}^\top - \widehat{\mathbf{U}}^{(m)}(\widehat{\mathbf{U}}^{(m)})^\top \right\|_2 \\ &\stackrel{\mathbb{P}}{\lesssim} \sqrt{Mn\lambda_{\max}} \cdot \frac{\mu\lambda_{\max}^{3/2}\sqrt{dn} \log^{3/2} n}{\delta^2} \\ &= \frac{\sqrt{M}\mu\lambda_{\max}^2\sqrt{dn}^{3/2} \log^{3/2} n}{\delta^2} \\ &\lesssim \mu\sqrt{M\lambda_{\max}d} \log^{5/2} n \end{aligned}$$

We now set about bounding the third term (17). Let $\mathbf{\Omega}_1 \mathbf{\Xi} \mathbf{\Omega}_2^\top$ denote a singular value decomposition of $(\widehat{\mathbf{U}}^{(m)})^\top \bar{\mathbf{U}}$, and set $\mathbf{W}^{(m)} := \mathbf{\Omega}_1 \mathbf{\Omega}_2^\top$. Let $\theta_i^{(m)}$ denote the principal angles between the column spaces of $\widehat{\mathbf{U}}^{(m)}$ and $\bar{\mathbf{U}}$ defined by $\xi_i^{(m)} = \cos(\theta_i^{(m)})$, where $\xi_i^{(m)}$ are the singular values of $(\widehat{\mathbf{U}}^{(m)})^\top \bar{\mathbf{U}}$. We invoke Wedin's theorem to show that

$$\begin{aligned} \left\| \mathbf{W}^{(m)} - (\widehat{\mathbf{U}}^{(m)})^\top \bar{\mathbf{U}} \right\|_2 &= \|\mathbf{I} - \mathbf{\Xi}\|_2 = \max_{i \in [d]} (1 - \xi_i^{(m)}) = \max_{i \in [d]} (1 - \cos \theta_i^{(m)}) \\ &\leq \max_{i \in [d]} (1 - \cos^2 \theta_i^{(m)}) = \max_{i \in [d]} \sin^2 \theta_i^{(m)} \lesssim \frac{\left\| \widehat{\mathbf{\Lambda}}^{(m)} - \bar{\mathbf{\Lambda}} \right\|_2^2}{(\sigma_d(\bar{\mathbf{\Lambda}}) - \sigma_{d+1}(\widehat{\mathbf{\Lambda}}))^2} \stackrel{\mathbb{P}}{\lesssim} \frac{Mn\lambda_{\max}}{M\delta^2} = \frac{n\lambda_{\max}}{\delta^2} \lesssim 1 \end{aligned}$$

We define $\mathbf{H}^{(m)} := \widehat{\mathbf{U}}^{(m)}(\widehat{\mathbf{U}}^{(m)})^\top - \mathbf{U}\mathbf{U}^\top$ and note that $\mathbf{H}^{(m)}$ is independent of $(\widehat{\mathbf{\Lambda}} - \bar{\mathbf{\Lambda}})_{\cdot,m}$, and

that

$$\begin{aligned}
\left\| \mathbf{H}^{(m)} \right\|_{2,\infty} &\leq \left\| \widehat{\mathbf{U}}^{(m)} \mathbf{W}^{(m)} - \bar{\mathbf{U}} \right\|_{2,\infty} + \left\| \widehat{\mathbf{U}}^{(m)} \right\|_{2,\infty} \left\| (\widehat{\mathbf{U}}^{(m)})^\top \bar{\mathbf{U}} - \mathbf{W}^{(m)} \right\|_2 \\
&\lesssim \left\| \widehat{\mathbf{U}}^{(m)} \mathbf{W}^{(m)} - \bar{\mathbf{U}} \right\|_{2,\infty} + \left\| \widehat{\mathbf{U}}^{(m)} \right\|_{2,\infty} \\
&\stackrel{\mathbb{P}}{\lesssim} \frac{\mu \lambda_{\max} \sqrt{dn} \log n}{\delta}
\end{aligned}$$

Then, using Lemma 4 we have that

$$\begin{aligned}
\left\| (\tilde{\mathbf{A}} - \bar{\mathbf{A}})_{\cdot, m}^\top \mathbf{H}^{(m)} \right\|_2 &\stackrel{\mathbb{P}}{\lesssim} M \log^2 n \left\| \mathbf{H}^{(m)} \right\|_{2,\infty} + \sqrt{\lambda_{\max} \log n} \left\| \mathbf{H}^{(m)} \right\|_{\mathbb{F}} \\
&\stackrel{\mathbb{P}}{\lesssim} \sqrt{M \log n \lambda_{\max}} \left\| \mathbf{H}^{(m)} \right\|_{2,\infty} + \sqrt{\lambda_{\max} d \log n} \left\| \mathbf{H}^{(m)} \right\|_2 \\
&\stackrel{\mathbb{P}}{\lesssim} \sqrt{M \log n \lambda_{\max}} \cdot \frac{\mu \lambda_{\max} \sqrt{dn} \log n}{\delta} + \sqrt{\lambda_{\max} d \log n} \frac{n \lambda_{\max}}{\delta} \\
&\leq \frac{\sqrt{M} \mu n \lambda_{\max}^{3/2} \sqrt{d} \log^{3/2} n}{\delta} \\
&\lesssim \mu \sqrt{M d \lambda_{\max}} \log^{5/2} n.
\end{aligned}$$

Combining these bounds and taking a union bound over $m \in [n]$, we have

$$\left\| (\widehat{\mathbf{A}} - \bar{\mathbf{A}})^\top (\widehat{\mathbf{U}} - \bar{\mathbf{U}} \mathbf{W}) \right\|_{2,\infty} \stackrel{\mathbb{P}}{\lesssim} \mu \sqrt{M d \lambda_{\max}} \log^{5/2} n,$$

and the term (10) is bounded as

$$\begin{aligned}
\left\| (\mathbf{I} - \bar{\mathbf{V}} \bar{\mathbf{V}}^\top) (\widehat{\mathbf{A}} - \bar{\mathbf{A}})^\top (\widehat{\mathbf{U}} - \bar{\mathbf{U}} \mathbf{W}) \right\|_{2,\infty} &\leq \left\| \mathbf{I} - \bar{\mathbf{V}} \bar{\mathbf{V}} \right\|_\infty \left\| (\widehat{\mathbf{A}} - \bar{\mathbf{A}})^\top (\widehat{\mathbf{U}} - \bar{\mathbf{U}} \mathbf{W}) \right\|_{2,\infty} \\
&\stackrel{\mathbb{P}}{\lesssim} \mu \sqrt{M \lambda_{\max} d} \log^{5/2} n.
\end{aligned}$$

Combining the bounds on (7)-(10), we have

$$\max_{i,j \in [n]} \sup_{t \in \mathcal{T}} \left\| \mathbf{W}_1 \widehat{Y}_i(t) - \bar{Y}_i(t) \right\|_2 = \left\| \widehat{\mathbf{V}} \widehat{\mathbf{S}} \mathbf{W}_1^\top - \bar{\mathbf{V}} \bar{\mathbf{S}} \right\|_{2,\infty} \stackrel{\mathbb{P}}{\lesssim} \mu \sqrt{M d \lambda_{\max}} \log^{5/2} n,$$

which completes the proof.

E.7 Controlling the bias term

E.7.1 Edge level bias

We begin by studying the edge-level bias of the histogram intensity estimator. Let $\rho_{ij}(t) = \int_0^t \lambda_{ij}(s) ds$ denote the cumulative intensity of edge i, j . Now we have, for $t \in B_\ell$,

$$\begin{aligned}
\mathbb{E} \left(\widehat{\lambda}_{ij}(t) \right) &= M \int_{B_\ell} \lambda_{ij}(s) dt \\
&= M \left\{ \rho_{ij} \left(\frac{\ell}{M} \right) - \rho_{ij} \left(\frac{\ell-1}{M} \right) \right\} \\
&= \frac{\rho_{ij} \left(\frac{\ell}{M} \right) - \rho_{ij} \left(\frac{\ell-1}{M} \right)}{\frac{\ell}{M} - \frac{\ell-1}{M}} \\
&= \lambda_{ij}(t^*)
\end{aligned}$$

for some $t^* \in B^\ell$, which follows by an application of the mean value theorem, where $\rho'(t) = \lambda_{ij}(t)$. We then apply the L -Lipschitz continuity of $\lambda_{ij}(t)$ to obtain

$$\begin{aligned} |\mathbb{E}(\widehat{\lambda}_{ij}(t)) - \widehat{\lambda}_{ij}(t)| &= |\lambda_{ij}(t^*) - \lambda_{ij}(t)| \\ &\leq L \cdot |t^* - t| \\ &\leq \frac{L}{M}. \end{aligned}$$

E.7.2 A subspace perturbation bound

Define the operator $\mathcal{A} : \mathbb{R}^n \rightarrow (\mathcal{T} \rightarrow \mathbb{R}^n)$ by

$$\mathcal{A}v(\cdot) = \int_{\mathcal{T}} \mathbf{\Lambda}(t)v(t) dt$$

and define the operator $\mathcal{A}^* : (\mathcal{T} \rightarrow \mathbb{R}^n) \rightarrow \mathbb{R}^n$ by

$$\mathcal{A}^*u = \mathbf{\Lambda}(\cdot)u.$$

Then $\Sigma \equiv \mathcal{A}\mathcal{A}^*$ since

$$\mathcal{A}\mathcal{A}^*u = \mathcal{A}(\mathbf{\Lambda}(\cdot)u) = \int_{\mathcal{T}} \mathbf{\Lambda}^2(t)u dt = \Sigma u.$$

Denote its eigenvalues $\sigma_1^2, \dots, \sigma_n^2$, and its corresponding orthonormal eigenvectors u_1, \dots, u_n , and define $v_i(\cdot) = \mathbf{\Lambda}(\cdot)u_i/\xi_i$ for all $i = 1, \dots, n$. Then, observe that $\mathbf{\Lambda}(\cdot)$ admits the (functional) singular value decomposition

$$\mathbf{\Lambda}(\cdot) = \sum_{i=1}^n \sigma_i u_i v_i(\cdot).$$

Define $\bar{\mathbf{A}}$ and its corresponding parameters analogously. Then by (a functional version of) Wedin's $\sin \Theta$ theorem

$$\|\bar{\mathbf{U}}\mathbf{W}_1 - \mathbf{U}\|_2 \lesssim \frac{\|\bar{\mathcal{L}} - \mathcal{L}\|_2}{\sigma_d - \sigma_{d+1}} \leq \frac{n \|\bar{\mathcal{L}} - \mathcal{L}\|_{\max}}{\sigma_d - \sigma_{d+1}} \leq \frac{nL}{M\delta}.$$

E.7.3 Controlling the bias term

Combining the above bounds, we have that uniformly for all i, j, t ,

$$\begin{aligned} \|\bar{Y}_i(t)\mathbf{W}_1 - Y_i(t)\|_2 &= \|\bar{\mathbf{A}}(t)\bar{\mathbf{U}}\mathbf{W}_1 - \mathbf{\Lambda}(t)\mathbf{U}\|_2 \\ &\leq \|\bar{\mathbf{A}}(t)\|_{2,\infty} \|\bar{\mathbf{U}}\mathbf{W}_1 - \mathbf{U}\|_2 + \|\bar{\mathbf{A}}(t) - \mathbf{\Lambda}(t)\|_{2,\infty} \|\mathbf{U}\|_2 \\ &\lesssim \frac{n^{3/2}\lambda_{\max}L}{M\delta} + \frac{\sqrt{n}L}{M} \\ &\leq \frac{n^{3/2}\lambda_{\max}L}{M\delta}, \end{aligned}$$

where the final inequality follows from the fact that $\delta \leq n\lambda_{\max}$.

F Proofs of the technical propositions

F.1 Proof of Proposition 2

We have that M^{-1} times the lower-triangular elements of each block of $\widehat{\mathbf{\Lambda}}$ are independent Poisson random variables with mean given by M^{-1} times the lower-triangular elements of each block of $\bar{\mathbf{\Lambda}}$. Define the matrices $\widehat{\mathbf{\Lambda}}^L$ and $\widehat{\mathbf{\Lambda}}^U$ with the upper and lower triangles, respectively, of each block set to zero, and the diagonals of each block halved, and define $\bar{\mathbf{\Lambda}}^L$ and $\bar{\mathbf{\Lambda}}^U$ similarly, so that $M^{-1}\widehat{\mathbf{\Lambda}}^L$

(respectively $M^{-1}\widehat{\mathbf{\Lambda}}^U$) has independent Poisson entries with means $M^{-1}\bar{\mathbf{\Lambda}}^L$ (respectively $M^{-1}\bar{\mathbf{\Lambda}}^U$), and $\widehat{\mathbf{\Lambda}} - \bar{\mathbf{\Lambda}} = (\widehat{\mathbf{\Lambda}}^L - \bar{\mathbf{\Lambda}}^L) + (\widehat{\mathbf{\Lambda}}^U - \bar{\mathbf{\Lambda}}^U)$.

We condition on the event that $(\widehat{\mathbf{\Lambda}}^L - \bar{\mathbf{\Lambda}}^L)_{ij} \lesssim M \log n$ for all i, j , which occurs with overwhelming probability by Lemma 3 and a union bound. Now, we employ Lemma 5 with $B := M \log n$ and $\nu := Mn\lambda_{\max}$ to obtain

$$\mathbb{P}\left(\left\|\widehat{\mathbf{\Lambda}}^L - \bar{\mathbf{\Lambda}}^L\right\|_2 \geq 4\sqrt{Mn\lambda_{\max}} + t\right) \leq n \exp\left(-\frac{t^2}{c(M \log n)^2}\right).$$

Setting $t = M \log^{3/2} n$, we have that

$$\left\|\widehat{\mathbf{\Lambda}}^L - \bar{\mathbf{\Lambda}}^L\right\|_2 \stackrel{\mathbb{P}}{\lesssim} \sqrt{Mn\lambda_{\max}} + M \log^{3/2} n \lesssim \sqrt{Mn\lambda_{\max}}$$

where the final inequality follows from Assumption 4. We obtain an analogous bound for $\left\|\widehat{\mathbf{\Lambda}}^U - \bar{\mathbf{\Lambda}}^U\right\|_2$ and combine the with the triangle inequality:

$$\left\|\widehat{\mathbf{\Lambda}} - \bar{\mathbf{\Lambda}}\right\|_2 \leq \left\|\widehat{\mathbf{\Lambda}}^L - \bar{\mathbf{\Lambda}}^L\right\|_2 + \left\|\widehat{\mathbf{\Lambda}}^U - \bar{\mathbf{\Lambda}}^U\right\|_2 \stackrel{\mathbb{P}}{\lesssim} \sqrt{Mn\lambda_{\max}}.$$

We now establish a bound on $\left\|\widehat{\mathbf{\Lambda}} - \bar{\mathbf{\Lambda}}\right\|_1$. We condition on the event $|\widehat{\mathbf{\Lambda}}_{ij} - \bar{\mathbf{\Lambda}}_{ij}| \lesssim M \log n$ for all i, j , which occurs with overwhelming probability due to Lemma 3 and a union bound, and note that we have $\sum_{j=1}^n \mathbb{E}(\widehat{\mathbf{\Lambda}}_{ji} - \bar{\mathbf{\Lambda}}_{ji})^2 \leq Mn\lambda_{\max}$. Then, by the classical Bernstein inequality we have for any $t > 0$,

$$\mathbb{P}\left\{\sum_{j=1}^n \left|\widehat{\mathbf{\Lambda}}_{ji} - \bar{\mathbf{\Lambda}}_{ji}\right| \geq t\right\} \leq 2 \exp\left\{\frac{-t^2}{2(Mn\lambda_{\max} + tM \log n/3)}\right\},$$

and setting $t = \sqrt{nM\lambda_{\max} \log n}$, we obtain

$$\sum_{j=1}^n \left|\widehat{\mathbf{\Lambda}}_{ji} - \bar{\mathbf{\Lambda}}_{ji}\right| \stackrel{\mathbb{P}}{\lesssim} \sqrt{nM\lambda_{\max} \log n}.$$

A union bound establishes that

$$\left\|\widehat{\mathbf{\Lambda}} - \bar{\mathbf{\Lambda}}\right\|_1 \stackrel{\mathbb{P}}{\lesssim} \sqrt{nM\lambda_{\max} \log n},$$

which establishes Proposition 2.

F.2 Proof of Proposition 3

Proposition 3 follows from an application of Weyl's inequality. We have

$$\sigma_1(\widehat{\mathbf{\Lambda}}) \leq \sigma_1(\bar{\mathbf{\Lambda}}) + |\sigma_1(\widehat{\mathbf{\Lambda}}) - \sigma_1(\bar{\mathbf{\Lambda}})| \leq \sigma_1(\bar{\mathbf{\Lambda}}) + \left\|\widehat{\mathbf{\Lambda}} - \bar{\mathbf{\Lambda}}\right\|_2 \stackrel{\mathbb{P}}{\lesssim} \sqrt{M\sigma_1(\mathbf{\Sigma})} + \sqrt{Mn\lambda_{\max}} \lesssim \sqrt{M\sigma_1(\mathbf{\Sigma})}$$

since $\sigma_1(\bar{\mathbf{\Lambda}}) = \sqrt{M\sigma_1(\mathbf{\Sigma})} \gtrsim \sqrt{M\delta} \gtrsim \sqrt{Mn\lambda_{\max}}$. Similarly we have

$$\sigma_d(\widehat{\mathbf{\Lambda}}) \geq \sigma_d(\bar{\mathbf{\Lambda}}) - |\sigma_1(\widehat{\mathbf{\Lambda}}) - \sigma_1(\bar{\mathbf{\Lambda}})| \geq \sigma_d(\bar{\mathbf{\Lambda}}) - \left\|\widehat{\mathbf{\Lambda}} - \bar{\mathbf{\Lambda}}\right\|_2 \stackrel{\mathbb{P}}{\gtrsim} \sqrt{M\sigma_d(\mathbf{\Sigma})} - \sqrt{Mn\lambda_{\max}} \gtrsim \sqrt{M\sigma_d(\mathbf{\Sigma})},$$

which establishes the proposition.

F.3 Proof of Proposition 4

We begin by constructing matrices $\bar{\mathbf{Q}}$ and $\bar{\mathbf{E}}$, via a symmetric dilation trick, such that the spectral norms of $\mathbf{Q}^\top(\hat{\mathbf{\Lambda}} - \bar{\mathbf{\Lambda}})\mathbf{R}$ and $\mathbf{Q}^\top\bar{\mathbf{E}}\bar{\mathbf{Q}}$ coincide, and then apply a classical ε -net argument to the spectral norm of $\bar{\mathbf{Q}}^\top\bar{\mathbf{E}}\bar{\mathbf{Q}}$, following the proof of Lemma D.1 in [15].

First, we set $\bar{\mathbf{E}} := \mathcal{D}(\hat{\mathbf{\Lambda}} - \bar{\mathbf{\Lambda}})$, where \mathcal{D} is the dilation operator (see Section E.2.1) and $\bar{\mathbf{Q}} = (\mathbf{Q} \mathbf{R})$, and observe that

$$\left\| \mathbf{Q}^\top (\hat{\mathbf{\Lambda}} - \bar{\mathbf{\Lambda}}) \mathbf{R} \right\|_2 = \left\| \bar{\mathbf{Q}}^\top \bar{\mathbf{E}} \bar{\mathbf{Q}} \right\|_2 = \max_{\|v\|_2 \leq 1} |v^\top \bar{\mathbf{Q}}^\top \bar{\mathbf{E}} \bar{\mathbf{Q}} v|$$

where the second equality follows from the Courant-Fischer min-max theorem. Now, let $\mathcal{S}_\varepsilon^{d-1}$ be an ε -net of the $d-1$ -dimensional unit sphere $\mathcal{S}^{d-1} := \{v : \|v\|_2 = 1\}$. By definition, for any $v \in \mathcal{S}^{d-1}$, there exists some $w(v) \in \mathcal{S}_\varepsilon^{d-1}$ such that $\|v - w(v)\|_2 < \varepsilon$ and

$$\begin{aligned} \left\| \bar{\mathbf{Q}}^\top \bar{\mathbf{E}} \bar{\mathbf{Q}} \right\|_2 &= \max_{\|v\|_2 \leq 1} |v^\top \bar{\mathbf{Q}}^\top \bar{\mathbf{E}} \bar{\mathbf{Q}} v| \\ &= \max_{\|v\|_2 \leq 1} \left| \{v^\top - w(v)^\top + w(v)^\top\} \bar{\mathbf{Q}}^\top \bar{\mathbf{E}} \bar{\mathbf{Q}} \{v - w(v) + w(v)\} \right| \\ &\leq (\varepsilon^2 + 2\varepsilon) \left\| \bar{\mathbf{Q}}^\top \bar{\mathbf{E}} \bar{\mathbf{Q}} \right\|_2 + \max_{w \in \mathcal{S}_\varepsilon^{d-1}} |w^\top \bar{\mathbf{Q}}^\top \bar{\mathbf{E}} \bar{\mathbf{Q}} w|. \end{aligned}$$

With $\varepsilon = 1/3$, we have

$$\left\| \bar{\mathbf{Q}}^\top \bar{\mathbf{E}} \bar{\mathbf{Q}} \right\|_2 \leq \frac{9}{2} \max_{w \in \mathcal{S}_{1/3}^{d-1}} |w^\top \bar{\mathbf{Q}}^\top \bar{\mathbf{E}} \bar{\mathbf{Q}} w|.$$

Now, $\mathcal{S}_{1/3}^{d-1}$ can be selected so that its cardinality can be upper bounded by $|\mathcal{S}_{1/3}^{d-1}| \leq 18^d$ (see, for example, [51]). For a fixed $w \in \mathcal{S}_{1/3}^{d-1}$, we let $z = \bar{\mathbf{Q}}w$ and note that since $\mathcal{S}_{1/3}^{d-1} \subset \mathcal{S}^{d-1}$, that $\|z\|_2 \leq 1$, and

$$|w^\top \bar{\mathbf{Q}}^\top \bar{\mathbf{E}} \bar{\mathbf{Q}} w| = \left| \sum_{i=1}^{n(M+1)} \sum_{j=1}^{n(M+1)} \bar{e}_{ij} z_i z_j \right| = 2 \left| \sum_{i=1}^n \sum_{j=1}^{nM} e_{ij} z_i z_{n+j} \right|$$

Now, over the event that entries $e_{ij} \lesssim M \log n$, for all i, j , which occurs with overwhelming probability by Lemma 3, Hoeffding's inequality and a union bound over $w \in \mathcal{S}_{1/3}^{d-1}$ gives

$$\begin{aligned} \mathbb{P} \left\{ \left\| \bar{\mathbf{Q}}^\top \bar{\mathbf{E}} \bar{\mathbf{Q}} \right\|_2 > t \right\} &\leq \sum_{w \in \mathcal{S}_{1/3}^{d-1}} \mathbb{P} \left(|w^\top \bar{\mathbf{Q}}^\top \bar{\mathbf{E}} \bar{\mathbf{Q}} w| > \frac{2t}{9} \right) \\ &= \sum_{w \in \mathcal{S}_{1/3}^{d-1}} \mathbb{P} \left\{ \left| \sum_{i=1}^n \sum_{j=1}^{nM} e_{ij} z_i z_{n+j} \right| > \frac{t}{9} \right\} \\ &\leq 2 \cdot 18^d \exp \left\{ -\frac{2t^2}{(9cM \log n)^2} \right\} \\ &= 2 \cdot \exp \left\{ d \log(18) - \frac{2t^2}{(9cM \log n)^2} \right\} \end{aligned}$$

Setting $t = M \log^{3/2} n$ gives

$$\left\| \mathbf{Q}^\top (\hat{\mathbf{\Lambda}} - \bar{\mathbf{\Lambda}}) \mathbf{R} \right\|_2 = \left\| \bar{\mathbf{Q}}^\top \bar{\mathbf{E}} \bar{\mathbf{Q}} \right\|_2 \stackrel{\mathbb{P}}{\lesssim} M \log^{3/2} n,$$

completing the proof.

F.4 Proof of Proposition 5

Denote the singular value decomposition of $\bar{\mathbf{U}}^\top \hat{\mathbf{U}}$ by $\mathbf{\Omega}_1 \mathbf{\Xi} \mathbf{\Omega}_2^\top$, where $\mathbf{\Xi} = \text{diag}(\xi_1, \dots, \xi_d)$, and let $\mathbf{W} := \mathbf{\Omega}_1 \mathbf{\Omega}_2^\top$. The principal angles $\{\theta_i\}_{i=1}^d$ between the column spaces of $\bar{\mathbf{U}}$ and $\hat{\mathbf{U}}$ are define by $\xi_i = \cos(\theta_i)$, and by the Wedin $\sin\Theta$ theorem, we have

$$\begin{aligned} \left\| \bar{\mathbf{U}}^\top \hat{\mathbf{U}} - \mathbf{W} \right\|_2 &= \left\| \mathbf{\Xi} - \mathbf{I} \right\|_2 = \max_{i \in [d]} |1 - \xi_i| = \max_{i \in [d]} |1 - \cos \theta_i| \leq \max_{i \in [d]} |1 - \cos^2 \theta_i| \\ &= \max_{i \in [d]} \sin^2 \theta_i \lesssim \frac{\|\hat{\mathbf{\Lambda}} - \bar{\mathbf{\Lambda}}\|_2^2}{(\sigma_d(\bar{\mathbf{\Lambda}}) - \sigma_{d+1}(\bar{\mathbf{\Lambda}}))^2} \stackrel{\mathbb{P}}{\lesssim} \frac{Mn\lambda_{\max}}{M\delta^2} = \frac{n\lambda_{\max}}{\delta^2} \lesssim \frac{\sqrt{n\lambda_{\max}}}{\delta}. \end{aligned} \quad (18)$$

We apply the Wedin $\sin\Theta$ theorem again to obtain a bound which we will require later:

$$\begin{aligned} \left\| \hat{\mathbf{U}} \hat{\mathbf{U}}^\top - \bar{\mathbf{U}} \bar{\mathbf{U}}^\top \right\|_2 \vee \left\| \hat{\mathbf{V}} \hat{\mathbf{V}}^\top - \bar{\mathbf{V}} \bar{\mathbf{V}}^\top \right\|_2 &= \left\| \sin \Theta \left(\hat{\mathbf{U}}, \bar{\mathbf{U}} \right) \right\|_2 \vee \left\| \sin \Theta \left(\hat{\mathbf{V}}, \bar{\mathbf{V}} \right) \right\|_2 \\ &\lesssim \frac{\|\hat{\mathbf{\Lambda}} - \bar{\mathbf{\Lambda}}\|_2}{\sigma_d(\bar{\mathbf{\Lambda}}) - \sigma_{d+1}(\bar{\mathbf{\Lambda}})} \\ &\stackrel{\mathbb{P}}{\lesssim} \frac{\sqrt{n\lambda_{\max}}}{\delta}. \end{aligned}$$

We now establish a bound on $\left\| \bar{\mathbf{U}}^\top \hat{\mathbf{U}} - \bar{\mathbf{V}}^\top \hat{\mathbf{V}} \right\|_2$. We start by showing that

$$\begin{aligned} \left\| \bar{\mathbf{U}}^\top \hat{\mathbf{U}} - \bar{\mathbf{V}}^\top \hat{\mathbf{V}} \right\|_2 &= \arg \max_{x: \|x\|_2 \leq 1} x^\top \left(\bar{\mathbf{U}}^\top \hat{\mathbf{U}} - \bar{\mathbf{V}}^\top \hat{\mathbf{V}} \right) x \\ &= \arg \max_{x: \|x\|_2 \leq 1} \sum_{i,j=1}^d x_i x_j \left(\bar{\mathbf{U}}^\top \hat{\mathbf{U}} - \bar{\mathbf{V}}^\top \hat{\mathbf{V}} \right)_{ij} \\ &\leq \arg \max_{x: \|x\|_2 \leq 1} \sum_{i,j=1}^d (1 + \bar{s}_i) x_i (1 + \bar{s}_j^{-1}) x_j \left(\bar{\mathbf{U}}^\top \hat{\mathbf{U}} - \bar{\mathbf{V}}^\top \hat{\mathbf{V}} \right)_{ij} \\ &= \arg \max_{x: \|x\|_2 \leq 1} \sum_{i,j=1}^d x^\top \left[\left(\bar{\mathbf{U}}^\top \hat{\mathbf{U}} - \bar{\mathbf{V}}^\top \hat{\mathbf{V}} \right) + \bar{\mathbf{S}} \left(\bar{\mathbf{U}}^\top \hat{\mathbf{U}} - \bar{\mathbf{V}}^\top \hat{\mathbf{V}} \right) \hat{\mathbf{S}}^{-1} \right] x \\ &= \left\| \left(\bar{\mathbf{U}}^\top \hat{\mathbf{U}} - \bar{\mathbf{V}}^\top \hat{\mathbf{V}} \right) + \bar{\mathbf{S}} \left(\bar{\mathbf{U}}^\top \hat{\mathbf{U}} - \bar{\mathbf{V}}^\top \hat{\mathbf{V}} \right) \hat{\mathbf{S}}^{-1} \right\|_2, \end{aligned}$$

and then we employ the decomposition

$$\begin{aligned} &\bar{\mathbf{U}}^\top \hat{\mathbf{U}} - \bar{\mathbf{V}}^\top \hat{\mathbf{V}} + \bar{\mathbf{S}} \left(\bar{\mathbf{U}}^\top \hat{\mathbf{U}} - \bar{\mathbf{V}}^\top \hat{\mathbf{V}} \right) \hat{\mathbf{S}}^{-1} \\ &= \left[\bar{\mathbf{U}}^\top \hat{\mathbf{U}} \hat{\mathbf{S}} - \bar{\mathbf{S}} \bar{\mathbf{V}}^\top \hat{\mathbf{V}} + \bar{\mathbf{S}} \bar{\mathbf{U}}^\top \hat{\mathbf{U}} - \bar{\mathbf{V}} \hat{\mathbf{V}} \right] \hat{\mathbf{S}}^{-1} \\ &= \left[\bar{\mathbf{U}}^\top \left(\hat{\mathbf{\Lambda}} - \bar{\mathbf{\Lambda}} \right) \hat{\mathbf{V}} + \bar{\mathbf{V}}^\top \left(\hat{\mathbf{\Lambda}} - \bar{\mathbf{\Lambda}} \right)^\top \bar{\mathbf{U}} \right] \hat{\mathbf{S}}^{-1} \\ &= \bar{\mathbf{U}}^\top \left(\hat{\mathbf{\Lambda}} - \bar{\mathbf{\Lambda}} \right) \left(\hat{\mathbf{V}} - \bar{\mathbf{V}} \bar{\mathbf{V}}^\top \hat{\mathbf{V}} \right) \hat{\mathbf{S}}^{-1} + \bar{\mathbf{U}}^\top \left(\hat{\mathbf{\Lambda}} - \bar{\mathbf{\Lambda}} \right) \bar{\mathbf{V}} \bar{\mathbf{V}}^\top \hat{\mathbf{V}} \hat{\mathbf{S}}^{-1} \\ &\quad + \bar{\mathbf{V}}^\top \left(\hat{\mathbf{\Lambda}} - \bar{\mathbf{\Lambda}} \right)^\top \left(\hat{\mathbf{U}} - \bar{\mathbf{U}} \bar{\mathbf{U}}^\top \hat{\mathbf{U}} \right) \hat{\mathbf{S}}^{-1} + \bar{\mathbf{V}}^\top \left(\hat{\mathbf{\Lambda}} - \bar{\mathbf{\Lambda}} \right)^\top \bar{\mathbf{U}} \bar{\mathbf{U}}^\top \hat{\mathbf{U}} \hat{\mathbf{S}}^{-1}. \end{aligned}$$

Therefore we have

$$\begin{aligned}
\left\| \bar{\mathbf{U}}^\top \hat{\mathbf{U}} - \bar{\mathbf{V}}^\top \hat{\mathbf{V}} \right\|_2 &\leq \left\| \hat{\mathbf{\Lambda}} - \bar{\mathbf{\Lambda}} \right\|_2 \left(\left\| \hat{\mathbf{V}} \hat{\mathbf{V}}^\top - \bar{\mathbf{V}} \bar{\mathbf{V}}^\top \right\|_2 + \left\| \hat{\mathbf{U}} \hat{\mathbf{U}}^\top - \bar{\mathbf{U}} \bar{\mathbf{U}}^\top \right\|_2 \right) \left\| \hat{\mathbf{S}}^{-1} \right\|_2 \\
&\quad \left\| \bar{\mathbf{U}}^\top (\hat{\mathbf{\Lambda}} - \bar{\mathbf{\Lambda}}) \bar{\mathbf{V}} \right\|_2 \left\| \hat{\mathbf{S}}^{-1} \right\|_2 + \left\| \bar{\mathbf{V}}^\top (\hat{\mathbf{\Lambda}} - \bar{\mathbf{\Lambda}})^\top \bar{\mathbf{U}} \right\|_2 \left\| \hat{\mathbf{S}}^{-1} \right\|_2 \\
&\stackrel{\mathbb{P}}{\lesssim} \sqrt{Mn\lambda_{\max}} \cdot \frac{\sqrt{n\lambda_{\max}}}{\delta} \cdot \frac{1}{\sigma_d(\bar{\mathbf{\Lambda}})} + \frac{M \log^{3/2} n}{\sigma_d(\bar{\mathbf{\Lambda}})} \\
&= \frac{n\lambda_{\max}}{\delta^2} + \frac{\sqrt{M} \log^{3/2} n}{\delta} \\
&\lesssim \frac{\sqrt{n\lambda_{\max}}}{\delta}.
\end{aligned}$$

Combining this with (18), we have

$$\left\| \bar{\mathbf{V}}^\top \hat{\mathbf{V}} - \mathbf{W} \right\|_2 \leq \left\| \bar{\mathbf{V}}^\top \hat{\mathbf{V}} - \bar{\mathbf{U}}^\top \hat{\mathbf{U}} \right\|_2 + \left\| \bar{\mathbf{U}}^\top \hat{\mathbf{U}} - \mathbf{W} \right\|_2 \stackrel{\mathbb{P}}{\lesssim} \frac{\sqrt{n\lambda_{\max}}}{\delta}.$$

F.5 Proof of Proposition 6

We begin by decomposing $\mathbf{W}\hat{\mathbf{S}} - \bar{\mathbf{S}}\mathbf{W}$ as

$$\begin{aligned}
\mathbf{W}\hat{\mathbf{S}} - \bar{\mathbf{S}}\mathbf{W} &= (\mathbf{W} - \bar{\mathbf{U}}^\top \hat{\mathbf{U}}) \hat{\mathbf{S}} + \bar{\mathbf{S}} (\mathbf{V}^\top \hat{\mathbf{V}} - \mathbf{W}) + \bar{\mathbf{U}}^\top \hat{\mathbf{U}} \hat{\mathbf{S}} - \bar{\mathbf{S}} \bar{\mathbf{V}}^\top \hat{\mathbf{V}} \\
&= (\mathbf{W} - \bar{\mathbf{U}}^\top \hat{\mathbf{U}}) \hat{\mathbf{S}} + \bar{\mathbf{S}} (\mathbf{V}^\top \hat{\mathbf{V}} - \mathbf{W}) + \bar{\mathbf{U}}^\top (\hat{\mathbf{\Lambda}} - \bar{\mathbf{\Lambda}}) \hat{\mathbf{V}} \\
&= (\mathbf{W} - \bar{\mathbf{U}}^\top \hat{\mathbf{U}}) \hat{\mathbf{S}} + \bar{\mathbf{S}} (\mathbf{V}^\top \hat{\mathbf{V}} - \mathbf{W}) + \bar{\mathbf{U}}^\top (\hat{\mathbf{\Lambda}} - \bar{\mathbf{\Lambda}}) (\hat{\mathbf{V}} \hat{\mathbf{V}}^\top - \bar{\mathbf{V}} \bar{\mathbf{V}}^\top) \hat{\mathbf{V}} \\
&\quad + \bar{\mathbf{U}}^\top (\hat{\mathbf{\Lambda}} - \bar{\mathbf{\Lambda}}) \bar{\mathbf{V}} \bar{\mathbf{V}}^\top \hat{\mathbf{V}},
\end{aligned}$$

and therefore we have that

$$\begin{aligned}
\left\| \mathbf{W}\hat{\mathbf{S}} - \bar{\mathbf{S}}\mathbf{W} \right\|_2 &\leq \left\| \mathbf{W} - \bar{\mathbf{U}}^\top \hat{\mathbf{U}} \right\|_2 \left\| \hat{\mathbf{\Lambda}} \right\|_2 + \left\| \mathbf{W} - \bar{\mathbf{V}}^\top \hat{\mathbf{V}} \right\|_2 \left\| \bar{\mathbf{\Lambda}} \right\|_2 \\
&\quad + \left\| \hat{\mathbf{\Lambda}} - \bar{\mathbf{\Lambda}} \right\|_2 \left\| \hat{\mathbf{V}} \hat{\mathbf{V}}^\top - \bar{\mathbf{V}} \bar{\mathbf{V}}^\top \right\|_2 + \left\| \bar{\mathbf{U}}^\top (\hat{\mathbf{\Lambda}} - \bar{\mathbf{\Lambda}}) \bar{\mathbf{V}} \right\|_2 \\
&\stackrel{\mathbb{P}}{\lesssim} \frac{\sqrt{n\lambda_{\max}} \kappa}{\delta} + \frac{\sqrt{M} n \lambda_{\max}}{\delta} + M \log^{3/2} n \\
&\lesssim M \log^{3/2} n,
\end{aligned}$$

which completes the proof.

F.6 Proof of Proposition 7

A key tool in proving Proposition 7 is a theorem due [13], providing entrywise eigenvector bounds for random matrices. The original statement is given for the eigenvectors of symmetric random matrices with row and columns-wise independence. We state a generalisation for the singular vectors of rectangular matrices with *block-wise* independence structure. The extension to block-wise independence structure has been handled in [14] (see Proposition 2.1(b) of that paper), although the exposition of the results in this paper are more complicated. For this reason, we choose to state the result due to [13] with this generalisation, which can be seen by following through the relevant parts of their proof.

Lemma 8 (A slight generalisation of Theorem 2.1 of [13]). *Let \mathbf{M}_0 be an $n_1 \times n_2$ real-valued random matrix. Define $n_0 = n_1 + n_2$ and let $\pi_1 = \sqrt{2n_1/n_0}$ and $\pi_2 = \sqrt{2n_2/n_0}$. Define $\kappa_0 := \sigma_1(\mathbf{E}\mathbf{M}_0)/\sigma_d(\mathbf{E}\mathbf{M}_0)$, $\delta_0 = \sigma_d(\mathbf{E}\mathbf{M}_0) - \sigma_{d+1}(\mathbf{E}\mathbf{M}_0)$. Suppose there exists some $\gamma > 0$ and a function $\varphi : \mathbb{R}_+ \rightarrow \mathbb{R}_+$ which is continuous and non-decreasing on \mathbb{R}_+ , with $\varphi(0) = 0$ and $\varphi(x)/x$ non-increasing on \mathbb{R}_+ , such that the following conditions hold:*

B1 (Incoherence). $\|\mathbb{E}\mathbf{M}_0\|_{2,\infty} \vee \|\mathbb{E}\mathbf{M}_0^\top\|_{2,\infty} \leq \gamma\delta_0$.

B2 (Block-wise independence). Assume that for any $k \in [n_1], \ell \in [n_2]$, there exists $\mathcal{N}_k^1 \subset [n_1]$ and $\mathcal{N}_\ell^2 \subset [n_2]$, such that the k th row of \mathbf{M}_0 is independent of the columns $\{j : j \notin \mathcal{N}_k^1\}$, and the ℓ th column of \mathbf{M}_0 is independent of the rows $\{i : i \notin \mathcal{N}_\ell^2\}$. Let $m_0 = \max_{k,\ell} \{|\mathcal{N}_k^1| \vee |\mathcal{N}_\ell^2|\}$ and assume $m_0 \lesssim \delta_0$.

B3 (Spectral norm concentration). $\kappa_0 \max\{\gamma, \varphi(\gamma)\} \lesssim 1$ and $\mathbb{P}(\|\mathbf{M}_0 - \mathbb{E}\mathbf{M}_0\|_2 > \gamma\Delta) \leq \eta_0$ for some $\eta_0 \in (0, 1)$.

B4. [Row and column concentration] There exists some $\eta_1 \in (0, 1)$ such that for any matrices $\mathbf{Q} \in \mathbb{R}^{n_1 \times d}, \mathbf{R} \in \mathbb{R}^{n_2 \times d}$ and $i \in [n_1], j \in [n_2]$,

$$\mathbb{P}\left\{\left\|\left(\mathbf{M}_0 - \mathbb{E}\mathbf{M}_0\right)_{\cdot,i} \mathbf{R}\right\|_2 \leq \delta_0 b_\infty \varphi\left(\frac{b_{\mathbb{F}}}{\sqrt{n_0} b_\infty}\right)\right\} \geq 1 - \frac{\eta_1}{n_0},$$

and

$$\mathbb{P}\left\{\left\|\left(\mathbf{M}_0 - \mathbb{E}\mathbf{M}_0\right)_{j,\cdot} \mathbf{Q}\right\|_2 \leq \delta_0 b_\infty \varphi\left(\frac{b_{\mathbb{F}}}{\sqrt{n_0} b_\infty}\right)\right\} \geq 1 - \frac{\eta_1}{n_0}$$

where $b_\infty := \pi_1 \|\mathbf{Q}\|_{2,\infty} \vee \pi_2 \|\mathbf{R}\|_{2,\infty}$, and $b_{\mathbb{F}} := (\pi_1 \|\mathbf{Q}\|_{\mathbb{F}}^2 + \pi_2 \|\mathbf{R}\|_{\mathbb{F}}^2)^{1/2}$.

Let $\widehat{\mathbf{U}}_0, \mathbf{U}_0$ (respectively $\widehat{\mathbf{V}}_0, \mathbf{V}_0$) be the matrices containing the left (respectively, right) singular vectors corresponding to the d leading singular values of \mathbf{M}_0 and $\mathbb{E}\mathbf{M}_0$. Then, with probability at least $1 - \eta_0 - 2\eta_1$, we have

$$\begin{aligned} \pi_1 \|\widehat{\mathbf{U}}_0\|_{2,\infty} \vee \pi_2 \|\widehat{\mathbf{V}}_0\|_{2,\infty} &\lesssim \{\kappa_0 + \varphi(1)\} (\pi_1 \|\mathbf{U}_0\|_{2,\infty} \vee \pi_2 \|\mathbf{V}_0\|_{2,\infty}) \\ &\quad + \gamma (\pi_1 \|\mathbb{E}\mathbf{M}_0\|_{2,\infty} \vee \pi_2 \|(\mathbb{E}\mathbf{M}_0)^\top\|_{2,\infty}) / \delta_0; \\ \pi_1 \|\widehat{\mathbf{U}}_0 \mathbf{O} - \mathbf{U}_0\|_{2,\infty} \vee \pi_2 \|\widehat{\mathbf{V}}_0 \mathbf{O} - \mathbf{V}_0\|_{2,\infty} &\lesssim [\kappa_0 \{\kappa_0 + \varphi(1)\} \{\gamma + \varphi(\gamma)\} + \varphi(1)] (\pi_1 \|\mathbf{U}_0\|_{2,\infty} \vee \pi_2 \|\mathbf{V}_0\|_{2,\infty}) \\ &\quad + \gamma (\pi_1 \|\mathbb{E}\mathbf{M}_0\|_{2,\infty} \vee \pi_2 \|(\mathbb{E}\mathbf{M}_0)^\top\|_{2,\infty}) / \delta_0. \end{aligned}$$

The following is an adaptation of Lemma D.2 of [15] (see also Lemma 7 of [13]) who showed an analogous result for Bernoulli random variables.

Lemma 9. Let $Y_i \sim \text{Poisson}(\lambda_i)$ independently for all $i = 1, \dots, n$, and suppose \mathbf{Q} is a deterministic matrix. The Q_i denote the i th row of \mathbf{Q} , and set $\lambda_{\max} := \max_{i \in [n]} \lambda_i$. Then for any $\alpha > 0$,

$$\mathbb{P}\left\{\left\|\sum_{i=1}^n (Y_i - \lambda_i) Q_i\right\| > \frac{(2 + \alpha)n\lambda_{\max} \|\mathbf{Q}\|_{2,\infty}}{1 \vee \log(\sqrt{n} \|\mathbf{Q}\|_{2,\infty} / \|\mathbf{Q}\|_{\mathbb{F}})}\right\} \leq 2de^{-\alpha n \lambda_{\max}}.$$

We omit the proof of Lemma 9, which is identical to the proof of Lemma D.2 of [15] with the Bernoulli moment generating function with the Poisson moment generating function.

With these tools to hand, we begin by obtaining a bound on $\|\widehat{\mathbf{U}}\|_{2,\infty}$ using Lemma 8, with $\mathbf{M}_0 := \widehat{\mathbf{A}}$. We set $\gamma := \sqrt{n\lambda_{\max}}/\delta$ and

$$\varphi(x) := \frac{n\lambda_{\max}}{\delta \{1 \vee \log(1/x)\}}.$$

First observe that $n_0 = n + nM \asymp nM$ and $\pi_1 \asymp M^{-1/2}$ and $\pi_2 \asymp 1$, and that $\kappa_0 = \kappa$ and $\delta_0 = \sqrt{M}\delta$. **B1** holds since $\|\widehat{\mathbf{A}}\|_{2,\infty} \leq \sqrt{n\lambda_{\max}} \lesssim \sqrt{n\lambda_{\max}}$ since $\lambda_{\max} \lesssim 1$ by Assumption 1. Using Assumptions 2 and 4, we have

$$M \lesssim \frac{n\lambda_{\max}}{\log^3 n} \lesssim \frac{\delta \log(\delta/\sqrt{n\lambda_{\max}})}{\kappa \log^3 n} \lesssim \frac{\delta \log n}{\kappa \log^3 n} \lesssim \delta,$$

and therefore **B2** holds. **B3** holds from Proposition 2, and observing that by Assumption 2, $\kappa_0 \max\{\gamma, \phi(\gamma)\} \lesssim 1$.

To see that **B4** holds, note that the each row and column of of $M^{-1}(\widehat{\mathbf{\Lambda}} - \bar{\mathbf{\Lambda}})$ contains independent Poisson random variables with means not exceeding $n\lambda_{\max}/M$. Then for $\mathbf{Q} \in \mathbb{R}^{n \times d}$, $\mathbf{R} \in \mathbb{R}^{nM \times d}$, setting $\alpha = \log n/n\lambda_{\max}$ in Lemma 9 implies that

$$\begin{aligned} \left\| \left(\widehat{\mathbf{\Lambda}} - \bar{\mathbf{\Lambda}} \right)_{i,\cdot} \mathbf{R} \right\|_{2,\infty} &= M \left\| \frac{1}{M} \left(\widehat{\mathbf{\Lambda}} - \bar{\mathbf{\Lambda}} \right)_{i,\cdot} \mathbf{R} \right\|_{2,\infty} \\ &\stackrel{\mathbb{P}}{\lesssim} M \cdot \frac{(n\lambda_{\max}/M + \log n) \|\mathbf{R}\|_{2,\infty}}{1 \vee \log \left(\frac{\sqrt{n_0} \|\mathbf{R}\|_{2,\infty}}{\|\mathbf{R}\|_{\mathbb{F}}} \right)} \\ &\lesssim \frac{n\lambda_{\max} \|\mathbf{R}\|_{2,\infty}}{1 \vee \log \left(\frac{\sqrt{n_0} \|\mathbf{R}\|_{2,\infty}}{\|\mathbf{R}\|_{\mathbb{F}}} \right)} \\ &= \delta \|\mathbf{R}\|_{2,\infty} \varphi \left(\frac{\|\mathbf{R}\|_{\mathbb{F}}}{\sqrt{n_0} \|\mathbf{R}\|_{2,\infty}} \right) \\ &\leq \delta_0 b_{\infty} \varphi \left(\frac{b_{\mathbb{F}}}{\sqrt{n_0} b_{\infty}} \right). \end{aligned}$$

Similarly, setting $\alpha = M \log n/n\lambda_{\max}$ we have

$$\left\| \left(\tilde{\mathbf{\Lambda}} - \bar{\mathbf{\Lambda}} \right)_{\cdot,i}^{\top} \mathbf{Q} \right\|_{2,\infty} \stackrel{\mathbb{P}}{\lesssim} \frac{\sqrt{M} n \lambda_{\max} \|\mathbf{Q}\|_{2,\infty}}{1 \vee \log \left(\sqrt{n_0} \|\mathbf{Q}\|_{2,\infty} / \|\mathbf{Q}\|_{\mathbb{F}} \right)} \leq \delta_0 b_{\infty} \varphi \left(\frac{\sqrt{n} b_{\infty}}{b_{\mathbb{F}}} \right),$$

which establishes **B4**. Having established **B1-B4**, we are ready to apply Lemma 8:

$$\left\| \widehat{\mathbf{U}} \right\|_{2,\infty} \stackrel{\mathbb{P}}{\lesssim} \sqrt{M} \{ \kappa_0 + \varphi(1) \} (\pi_1 \|\mathbf{U}\|_{2,\infty} \vee \pi_2 \|\mathbf{V}\|_{2,\infty}) + \sqrt{M} \gamma \left(\pi_1 \|\bar{\mathbf{\Lambda}}\|_{2,\infty} \vee \pi_2 \|\bar{\mathbf{\Lambda}}^{\top}\|_{2,\infty} \right) / \delta_0$$

We have

$$\begin{aligned} \|\bar{\mathbf{V}}\|_{2,\infty} &= \|\bar{\mathbf{\Lambda}} \bar{\mathbf{U}} \bar{\mathbf{S}}^{-1}\|_{2,\infty} \leq \|\bar{\mathbf{\Lambda}}\|_{\infty} \|\bar{\mathbf{U}}\|_{2,\infty} \|\bar{\mathbf{S}}\|_2^{-1} \lesssim \frac{n\lambda_{\max} \mu \sqrt{d/n}}{\sigma_d^{1/2}(\mathbf{\Sigma})} \\ &\lesssim \frac{n\lambda_{\max} \mu \sqrt{d/n}}{\sqrt{M} \delta} \lesssim \sqrt{\frac{d}{nM}} \mu \log n. \end{aligned} \tag{19}$$

where we used Assumption 2 in the final inequality. Therefore

$$\pi_1 \|\bar{\mathbf{U}}\|_{2,\infty} \vee \pi_2 \|\bar{\mathbf{V}}\|_{2,\infty} \leq \sqrt{\frac{d}{nM}} \mu \log n,$$

and we have

$$\kappa = \frac{\sigma_1^{1/2}(\mathbf{\Sigma})}{\sigma_d^{1/2}(\mathbf{\Sigma})} \lesssim \frac{n\lambda_{\max}}{\delta} = \varphi(1)$$

and so the first term satisfies

$$\begin{aligned} \sqrt{M} \{ \kappa_0 + \varphi(1) \} (\pi_1 \|\mathbf{U}\|_{2,\infty} \vee \pi_2 \|\mathbf{V}\|_{2,\infty}) &\lesssim \sqrt{M} \varphi(1) (\pi_1 \|\mathbf{U}\|_{2,\infty} \vee \pi_2 \|\mathbf{V}\|_{2,\infty}) \\ &\lesssim \sqrt{M} \cdot \frac{n\lambda_{\max}}{\delta} \cdot \sqrt{\frac{d}{nM}} \mu \log n \\ &= \frac{\mu \lambda_{\max} \sqrt{nd} \log n}{\delta}. \end{aligned}$$

To control the second term, we first observe that

$$\begin{aligned} \pi_1 \|\bar{\mathbf{\Lambda}}\|_{2,\infty} &\leq M^{-1/2} \|\bar{\mathbf{U}} \bar{\mathbf{U}}^{\top} \bar{\mathbf{\Lambda}}\|_{2,\infty} + M^{-1/2} \|(\mathbf{I} - \bar{\mathbf{U}} \bar{\mathbf{U}}) \bar{\mathbf{\Lambda}}\|_{2,\infty} \\ &\lesssim M^{-1/2} \|\bar{\mathbf{U}}\|_{2,\infty} \|\bar{\mathbf{\Lambda}}\|_2 + M^{-1/2} \max_{i \in [n]} \sup_{t \in (0,1]} r_i(t) \\ &\lesssim \sqrt{\frac{d}{Mn}} \mu \cdot \sqrt{M} \kappa \delta + \mu \sqrt{d \lambda_{\max}} \log^{5/2} n \\ &\lesssim \mu \delta \sqrt{d \lambda_{\max}} \end{aligned}$$

where the final inequality follows from $\kappa \lesssim \log n \leq \sqrt{n}$ and $\lambda_{\max} \lesssim 1$. Similarly we obtain $\pi_2 \|\bar{\mathbf{\Lambda}}^\top\|_{2,\infty} \lesssim \mu\delta\sqrt{d\lambda_{\max}} \log n$ using (19), and therefore

$$\pi_1 \|\bar{\mathbf{\Lambda}}\|_{2,\infty} \vee \pi_2 \|\bar{\mathbf{\Lambda}}^\top\|_{2,\infty} \lesssim \mu\delta\sqrt{d\lambda_{\max}} \log n.$$

We then have

$$\begin{aligned} \sqrt{M}\gamma \left(\pi_1 \|\bar{\mathbf{\Lambda}}\|_{2,\infty} \vee \pi_2 \|\bar{\mathbf{\Lambda}}^\top\|_{2,\infty} \right) / \delta_0 &\lesssim \sqrt{M} \cdot \frac{\sqrt{n\lambda_{\max}}}{\delta} \cdot \mu\delta\sqrt{d\lambda_{\max}} \log n \cdot \frac{1}{\sqrt{M}\delta} \\ &\lesssim \frac{\mu\sqrt{nd\lambda_{\max}} \log n}{\delta}. \end{aligned}$$

Combining these bounds, we obtain

$$\|\hat{\mathbf{U}}\|_{2,\infty} \stackrel{\mathbb{P}}{\lesssim} \frac{\mu\sqrt{nd\lambda_{\max}} \log n}{\delta}.$$

We now apply Lemma 8 with $\mathbf{M}_0 = \hat{\mathbf{\Lambda}}^{(m)}$. We set γ and $\varphi(x)$ as before and verify Assumptions **B1-B4** in the same way. By analogous calculations to the above, we obtain the bound

$$\|\hat{\mathbf{U}}^{(m)}\|_{2,\infty} \stackrel{\mathbb{P}}{\lesssim} \frac{\mu\sqrt{nd\lambda_{\max}} \log n}{\delta}.$$

The final bound is shown in the same way, requiring the additional observation that $\kappa \{\gamma \vee \varphi(\gamma)\} \lesssim 1$ which follows from Assumption 2, and we obtain

$$\begin{aligned} \pi_1 \|\hat{\mathbf{U}}_0 \mathbf{O} - \mathbf{U}_0\|_{2,\infty} \vee \pi_2 \|\hat{\mathbf{V}}_0 \mathbf{O} - \mathbf{V}_0\|_{2,\infty} \\ &\stackrel{\mathbb{P}}{\lesssim} [\kappa_0 \{\kappa_0 + \varphi(1)\} \{\gamma + \varphi(\gamma)\} + \varphi(1)] (\pi_1 \|\mathbf{U}_0\|_{2,\infty} \vee \pi_2 \|\mathbf{V}_0\|_{2,\infty}) + \gamma \left(\pi_1 \|\bar{\mathbf{\Lambda}}\|_{2,\infty} \vee \pi_2 \|\bar{\mathbf{\Lambda}}^\top\|_{2,\infty} \right) / \delta_0 \\ &\lesssim \varphi(1) (\pi_1 \|\mathbf{U}_0\|_{2,\infty} \vee \pi_2 \|\mathbf{V}_0\|_{2,\infty}) + \gamma \left(\pi_1 \|\bar{\mathbf{\Lambda}}\|_{2,\infty} \vee \pi_2 \|\bar{\mathbf{\Lambda}}^\top\|_{2,\infty} \right) / \delta_0 \\ &\lesssim \frac{\mu\sqrt{nd\lambda_{\max}} \log n}{\delta} \end{aligned}$$

F.7 Proof of Proposition 8

We show (12) using a simple application of Wedin's inequality:

$$\begin{aligned} \|\hat{\mathbf{U}}^{(m)} (\hat{\mathbf{U}}^{(m)})^\top - \bar{\mathbf{U}} \bar{\mathbf{U}}^\top\|_2 &= \|\sin \Theta \left(\hat{\mathbf{U}}^{(m)}, \bar{\mathbf{U}} \right)\|_2 \lesssim \frac{\|\hat{\mathbf{\Lambda}}^{(m)} - \bar{\mathbf{\Lambda}}\|_2}{\sigma_d(\bar{\mathbf{\Lambda}}) - \sigma_{d+1}(\bar{\mathbf{\Lambda}})} \leq \frac{\|\hat{\mathbf{\Lambda}} - \bar{\mathbf{\Lambda}}\|_2}{\sigma_d(\bar{\mathbf{\Lambda}}) - \sigma_{d+1}(\bar{\mathbf{\Lambda}})} \\ &\stackrel{\mathbb{P}}{\lesssim} \frac{\sqrt{Mn\lambda_{\max}}}{\sqrt{M}\delta} = \frac{\sqrt{n\lambda_{\max}}}{\delta}. \end{aligned}$$

The proof of (13) requires a more delicate argument. We apply Wedin's theorem to obtain

$$\|\hat{\mathbf{U}}^{(m)} (\hat{\mathbf{U}}^{(m)})^\top - \hat{\mathbf{U}} \hat{\mathbf{U}}^\top\|_2 = \|\sin \Theta \left(\hat{\mathbf{U}}^{(m)}, \hat{\mathbf{U}} \right)\|_2 \lesssim \frac{\left\| \left(\hat{\mathbf{\Lambda}}^{(m)} - \hat{\mathbf{\Lambda}} \right)^\top \hat{\mathbf{U}}^{(m)} \right\|_2 \vee \left\| \left(\hat{\mathbf{\Lambda}}^{(m)} - \hat{\mathbf{\Lambda}} \right) \hat{\mathbf{V}}^{(m)} \right\|_2}{\sigma_d(\hat{\mathbf{\Lambda}}) - \sigma_{d+1}(\hat{\mathbf{\Lambda}})}. \quad (20)$$

By Weyl's inequality

$$\sigma_d(\hat{\mathbf{\Lambda}}) \geq \sigma_d(\bar{\mathbf{\Lambda}}) + \|\hat{\mathbf{\Lambda}} - \bar{\mathbf{\Lambda}}\|_2 \stackrel{\mathbb{P}}{\gtrsim} \sigma_d(\bar{\mathbf{\Lambda}}).$$

and

$$\sigma_{d+1}(\hat{\mathbf{\Lambda}}) \leq \sigma_{d+1}(\bar{\mathbf{\Lambda}}) - \|\hat{\mathbf{\Lambda}} - \bar{\mathbf{\Lambda}}\|_2 \stackrel{\mathbb{P}}{\lesssim} \sigma_{d+1}(\bar{\mathbf{\Lambda}}).$$

and therefore

$$\sigma_d(\widehat{\mathbf{\Lambda}}) - \sigma_{d+1}(\widehat{\mathbf{\Lambda}}) \stackrel{\mathbb{P}}{\gtrsim} \sigma_d(\bar{\mathbf{\Lambda}}) - \sigma_{d+1}(\bar{\mathbf{\Lambda}}) = \sqrt{M} \left(\sigma_d^{1/2}(\mathbf{\Sigma}) - \sigma_{d+1}^{1/2}(\mathbf{\Sigma}) \right) = \sqrt{M}\delta. \quad (21)$$

We now focus our attention on obtaining a bound for $\|(\widehat{\mathbf{\Lambda}}^{(m)} - \widehat{\mathbf{\Lambda}})\widehat{\mathbf{U}}^{(m)}\|_{\text{F}}$. Let

$$\mathcal{N}_m = \{m + (\ell - 1)n, \ell \in [M]\}.$$

The ij th entry of $\widehat{\mathbf{\Lambda}} - \widehat{\mathbf{\Lambda}}^{(m)}$ is

$$\left(\widehat{\mathbf{\Lambda}}^{(m)} - \widehat{\mathbf{\Lambda}}\right)_{ij} = \left(\widehat{\mathbf{\Lambda}}^{(m)} - \bar{\mathbf{\Lambda}}\right)_{ij} \mathbb{I}(i = m, j \in \mathcal{N}_m),$$

and so $\widehat{\mathbf{\Lambda}}^{(m)} - \widehat{\mathbf{\Lambda}}$ is independent of $\widehat{\mathbf{\Lambda}}^{(m)}$ and hence $\widehat{\mathbf{\Lambda}}^{(m)} - \widehat{\mathbf{\Lambda}}$ is independent of $\widehat{\mathbf{U}}^{(m)}$. We can then write

$$\begin{aligned} \left\| \left(\widehat{\mathbf{\Lambda}}^{(m)} - \widehat{\mathbf{\Lambda}}\right)^\top \widehat{\mathbf{U}}^{(m)} \right\|_{\text{F}}^2 &= \sum_{\ell \notin \mathcal{N}_m} \left(\widehat{\mathbf{\Lambda}}_{m,\ell} - \bar{\mathbf{\Lambda}}_{m,\ell}\right)^2 \left\| \widehat{\mathbf{U}}_{\ell,\cdot}^{(m)} \right\|_2^2 \\ &\quad + \left\| \sum_{\ell \in \mathcal{N}_m} \sum_{i=1}^n \left(\widehat{\mathbf{\Lambda}}_{i\ell} - \bar{\mathbf{\Lambda}}_{i\ell}\right) \widehat{\mathbf{U}}_{\ell,\cdot}^{(m)} \right\|_2^2 \\ &=: \zeta_1 + \zeta_2. \end{aligned}$$

The (square root of the) first term is easily bounded as

$$\begin{aligned} \zeta_1^{1/2} &\leq \left\| \widehat{\mathbf{\Lambda}} - \bar{\mathbf{\Lambda}} \right\|_{2,\infty} \left\| \widehat{\mathbf{U}}^{(m)} \right\|_{2,\infty} \\ &\leq \left\| \widehat{\mathbf{\Lambda}} - \bar{\mathbf{\Lambda}} \right\|_2 \left\| \widehat{\mathbf{U}}^{(m)} \right\|_{2,\infty} \\ &\stackrel{\mathbb{P}}{\lesssim} \sqrt{Mn\lambda_{\max}} \cdot \frac{\mu\sqrt{nd}\lambda_{\max}\log n}{\delta} \\ &= \frac{\sqrt{Mdn}\lambda_{\max}^{3/2}\mu\log n}{\delta} \end{aligned}$$

and to bound the second term, we employ Lemma 4 to obtain

$$\begin{aligned} \zeta_2^{1/2} &\stackrel{\mathbb{P}}{\lesssim} M\log^2 n \left\| \widehat{\mathbf{U}}^{(m)} \right\|_{2,\infty} + \sqrt{M\lambda_{\max}\log n} \left\| \widehat{\mathbf{U}}^{(m)} \right\|_{\text{F}} \\ &\leq M\log^2 n \left\| \widehat{\mathbf{U}}^{(m)} \right\|_{2,\infty} + \sqrt{M\lambda_{\max}n\log n} \left\| \widehat{\mathbf{U}}^{(m)} \right\|_{2,\infty} \\ &\lesssim \sqrt{M\lambda_{\max}n\log n} \left\| \widehat{\mathbf{U}}^{(m)} \right\|_{2,\infty} \\ &\lesssim \sqrt{M\lambda_{\max}n\log n} \cdot \frac{\mu\sqrt{nd}\lambda_{\max}\log n}{\delta} \\ &= \frac{\sqrt{Mdn}\lambda_{\max}^{3/2}\mu\log^{3/2} n}{\delta} \end{aligned}$$

where we used Assumption 4 in the third inequality. Therefore

$$\left\| \left(\widehat{\mathbf{\Lambda}}^{(m)} - \widehat{\mathbf{\Lambda}}\right)^\top \widehat{\mathbf{U}}^{(m)} \right\|_2 \leq \left\| \left(\widehat{\mathbf{\Lambda}}^{(m)} - \widehat{\mathbf{\Lambda}}\right)^\top \widehat{\mathbf{U}}^{(m)} \right\|_{\text{F}} \leq \zeta_1^{1/2} + \zeta_2^{1/2} \stackrel{\mathbb{P}}{\lesssim} \frac{\sqrt{Mdn}\lambda_{\max}^{3/2}\mu\log^{3/2} n}{\delta}.$$

Similar analysis yields an analogous bound for $\|(\widehat{\mathbf{\Lambda}}^{(m)} - \widehat{\mathbf{\Lambda}})\widehat{\mathbf{V}}^{(m)}\|_2$, and combining this, with (20)

and (21) we have

$$\begin{aligned} \left\| \widehat{\mathbf{U}}^{(m)} (\widehat{\mathbf{U}}^{(m)})^\top - \widehat{\mathbf{U}} \widehat{\mathbf{U}}^\top \right\|_2 &\lesssim \frac{\left\| (\widehat{\mathbf{\Lambda}}^{(m)} - \widehat{\mathbf{\Lambda}})^\top \widehat{\mathbf{U}}^{(m)} \right\|_2 \vee \left\| (\widehat{\mathbf{\Lambda}}^{(m)} - \widehat{\mathbf{\Lambda}}) \widehat{\mathbf{V}}^{(m)} \right\|_2}{\sigma_d(\widehat{\mathbf{\Lambda}}) - \sigma_{d+1}(\widehat{\mathbf{\Lambda}})} \\ &\stackrel{\mathbb{P}}{\lesssim} \frac{\sqrt{dn} \lambda_{\max}^{3/2} \mu \log^{3/2} n}{\delta^2} \end{aligned}$$

which establishes the proposition.